THE EFFECT OF BULK DENSITY ON DEBRIS FLOW MOBILIZATION, MARIN COUNTY, CA

A thesis submitted to the faculty of
San Francisco State University
In partial fulfillment of
the requirements for
the Degree

Master of Science

In

Geosciences

by

Shawn Wesley Henderson

San Francisco, California

Summer 2016

CERTIFICATION OF APPROVAL

I certify that I have read THE EFFECT OF BULK DENSITY ON DEBRIS FLOW MOBILIZATION, MARIN COUNTY, CA by Shawn Wesley Henderson, and that in my opinion this work meets the criteria for approving a thesis submitted in partial fulfillment of the requirement for the degree Master of Science: Geoscience at San Francisco State University.

Leonard Sklar, Ph.D
Professor of Earth & Climate Sciences

Jonathan Stock, Ph.D
United States Geological Survey

Daniel P. Dempsey (for Karen Grove

Karen Grove, Ph.D
Professor Emerita Earth & Climate Sciences

THE EFFECT OF BULK DENSITY ON DEBRIS FLOW

MOBILIZATION, MARIN COUNTY, CA

Shawn Wesley Henderson
San Francisco, California
2016

I tested the hypothesis that soils with low bulk density are more likely to mobilize into a debris flow during a shallow landslide event. Laboratory tests have demonstrated that loose, low bulk density soils contract during deformation causing elevated pore pressures and liquefaction. This mechanism for debris flow mobilization is not observed in the densest soils which fail as slump blocks. Previous methods of measuring bulk density are time consuming and imprecise, making them inadequate for testing this idea in the field. I measured bulk density using an instrument called the Mold Impression Laser Tool (MILT), a portable 3D scanner developed by NASA and modified by USGS for field measurement of soil density. Using the MILT, I performed bulk density measurements in soils adjacent to 15 shallow landslide scars in Marin County and compared the density of soil at debris flows sites to soil at slump sites. The average bulk density of debris flows (1.341 +/- 0.046 g/cm^3; mean +/- S.E.) was significantly lower than the density of slumps (1.604 +/- 0.016 g/cm^3; mean+/- S.E.) and the critical bulk density that separated mobilized failures from slumps was between 1.48 g/cm^3 and 1.57 g/cm^3. These findings suggest that slopes susceptible to debris flows can be identified by measuring soil bulk density.

I certify that the Abstract is a correct representation of the content of this Thesis

Chair, Thesis Committee

August 4, 2016
Date

ACKNOWLEDGEMENTS

First and foremost, I would like to thank my committee for their unique and indispensable contributions to this project. I thank Leonard Sklar for his optimism, mastery of statistics and injections of excitement to this project at every step of the way. I thank Jonathan Stock for sharing unpublished mapping of Marin and San Francisco landslides and debris flows, field training, introducing me to landslides and the MILT and for the initial vision for this project. Lastly, I thank Karen Grove for her generosity, unrivaled editing and for being my mentor for my years at SF State. In addition, I would like to thank Dave Dempsey and Russell McArthur, two members of the SF State Earth & Climate Sciences Department who assisted me through administrative and logistical hurtles.

I would also like to send my love and gratitude to my family, in particular my mom, dad, Aunt Barbara and my fiancé, Lauren who have supported me during this long journey of going back to school.

This project would not have been possible without the funding from the Dawdy Research Grant and the Grove-Ach Fellowship. These contributions were truly generous and demonstrate a commitment to scientific progress and the achievement of students such as myself.

TABLE OF CONTENTS

LIST OF TABLES

LIST OF FIGURES

LIST OF APPENDICES

Appendix Page

1.0 INTRODUCTION

In the San Francisco Bay Area (fig. 1), shallow landslides are common during periods of heavy rainfall. These landslides are hazardous, causing extensive property damage and even fatalities. During a particularly intense storm in 1982, shallow landslides were responsible for at least $66 million in damages and 25 deaths (Ellen and Wieczorek, 1988). Much damage was caused by shallow landslides that mobilized into debris flows (fig. 2), mixtures of rock, water and soil that are far-traveled and dangerous. A smaller number of landslides failed as rotational slumps, and did not mobilize (fig. 3; Cruden and Varnes, 1996).

The damage from the 1982 storm highlighted the hazard of debris flows that mobilize from relatively small, shallow landslides (Nilsen et al., 1979; Ellen and Wieczorek, 1988). In response to this and other storms, researchers focused on improving our ability to predict when and where shallow landslides are likely to occur. This study explores the hypothesis that measurable variations in soil density co-vary with failure mode. Specifically, I test the hypothesis that soils that fail as slumps are measurably denser than those that mobilize into debris flows. Testing this hypothesis opens the door to our ability to forecast how soils will fail during large storms in Marin County (fig. 1) and elsewhere.

Previous laboratory tests suggest that a soil's bulk density (the dry mass of the soil per unit volume) influences whether a soil is likely to mobilize into a debris flow or slump during a shallow landslide (Casagrande, 1975; Ellen and Flemming, 1987; Iverson et al., 2000). In a laboratory setting, researchers have demonstrated that loose, low bulk density soil is more likely to mobilize into a debris flow (Iverson et al., 2000). This hypothesis is harder to test in the field because

1) you need a technique that is field portable and accurate
2) you need a large data set of landslides that failed in different modes

Conventional field measurements of bulk density are difficult and time consuming (Heuscher et al., 2005; Benites, 2007). For this reason, the common sampling protocol is to take a single measurement in the headscarp, half way between the surface and the failure plane (Gabet and Mudd, 2006, Mckenna et al., 2012). This is problematic because it uses only a small sample to represent the density of the entire failed material. Furthermore, previous studies have demonstrated that various methods of measurement (core method, excavation method, radiation method) produce conflicting bulk density values when deployed on the same soil. Some of these values differ from each other as much as 37% (Page-Dumroese et al., 1999). This is mainly due to the issue of soil compaction while taking cores, which is the most common method for measuring bulk density (Blake, 1965; Page-Dumroese et al., 1999, Miller et al., 2001).

Other methods of measuring bulk density, which are used less frequently, are also problematic. The excavation method requires excavation of a soil sample which is baked to drive off moisture and weighed to determine mass. The volume of the soil sample is determined by using a sandcone or a plastic lining to fill the hole with a known volume of sand or water, respectively. (Blake, 1965; Page-Dumroese et al., 1999, Miller et al., 2001). These techniques do not, however, take into account irregularities in the soil surface which is assumed to be flat. In addition, sand is compressible and can lead to imprecise volume measurements as grains pack variably. The radiation method gives immediate results and requires no excavation, but is impractical for field use because of its weight and the user needs to be certified to handle radioactive material (Page-Dumroese et al., 1999). Because of these issues with conventional bulk density measurement (core, excavation and radiation methods), I took advantage of a new field method of measuring bulk density using the Mold Impression Laser Tool (MILT; fig. 4).

The MILT is a portable, 3D scanner developed by NASA to quantitatively evaluate surface defects from damage to the heat shield of the space shuttle (Lavelle et al., 2007). Dr. Jonathan Stock, United States Geologic Survey (USGS), Research Geologist & Director, USGS Innovation Center, worked with NASA to repurpose the MILT to make precise measurements of soil bulk density. The team developed custom software and designed a platform for precise measurements of soil volume. The MILT is battery-powered, lightweight and connects wirelessly to a laptop or tablet, making it suitable for fieldwork.

Using Stock's unpublished map of 2006 and 1982 shallow failures in Marin County, I visited mapped failures with the MILT to take bulk density measurements from soils adjacent to shallow landslide scars throughout Marin County and San Francisco (fig. 1). The MILT allows a user to estimate soil volume changes with high accuracy and precision with a few seconds of scanning. This change in soil volume, along with the mass of the excavated soil, is used to calculate the bulk density of the excavated soil sample. With this new method of measuring bulk density, I avoided the issues associated with conventional methods of bulk density measurements, thus improving the accuracy and precision of the measurements. I also performed multiple measurements per landslide to produce a more representative density for the soil at each slide. I used this improved method to compare the density of soils adjacent to landslides that mobilized into debris flows to soils adjacent to landslides that did not. I also tested the effect of soil bulk density on mapped debris flow runout length. In the course of this work, I characterized the spatial variability of soil density around shallow landslide scarps, and with depth.

2.0 BACKGROUND

Considerable research has focused on the link between soil bulk density and debris flow mobilization. Contraction of loose, low bulk density soil is thought to cause liquefaction during soil failure and cause the soil to mobilize downslope as a debris flow. Dense, high bulk density soil dilates during deformation and is thought to inhibit soil movement, causing the material to travel slowly downslope as a slump (Ellen and Flemming, 1987; Iverson et al., 1997; Iverson et al., 2000, Gabet and Mudd, 2006, Mckenna et al., 2016). In a laboratory setting, flume studies (Iverson et al., 2000) have supported this idea, but field studies such as Gabet and Mudd (2006) and Mckenna et al (2016) did not reproduce laboratory findings. This may be due to inadequacies of conventional bulk density measurement. The following sections explain the mechanics of landslide activation, the role of density in landslide failure mode (e.g., slump versus mobilizing into a debris flow), and the challenges with interpreting previous studies.

2.1 Landslide and Debris Flow Mechanics

Shallow landslides occur on steep slopes where a thin, granular soil mantle overlies bedrock (Ellen and Flemming, 1987). During heavy rainfall, water accumulates in the soil at horizons with infiltration rates that are lower than rainfall rates. This is often, but not always, the interface between the lower-permeability bedrock and higher-permeability soil mantle (Ellen and Flemming, 1987). Ponding can also occur at sites of strong conductivity contrasts between soil horizons or strata, such as the contact between a clay-rich horizon and an overlying sand-rich horizon (Ellen and Flemming, 1987). In many steeplands, these shallow-type landslides preferentially occur in hollows, which are concave areas of the topography that collect and concentrate rainwater from a large drainage area

(Wilson et al., 1986). This build-up of water within the soil ultimately causes the slope to fail.

A landslide occurs when the force of gravity exceeds the strength of the soil. A soil's shear strength has at least two components: friction and cohesion. Friction depends on the effective normal stress applied to the soil by the overlying material and is inversely proportional to the angle of the hillslope (Duncan, 1996). On gentle slopes, effective normal stress is high, increasing friction between grains and increasing slope stability, whereas on steep slopes, effective normal stress is lower, reducing friction and contributing to slope instability (Duncan, 1996). Cohesion, on the other hand, is the intrinsic strength of the material and is unaffected by effective normal stress (Duncan, 1996). Soils that have undergone cementation or that have high clay content are generally more cohesive, as are soils with dense root networks.

During or shortly after a storm, rainwater may pond at a low conductivity horizon or contact with the underlying bedrock. This water increases the pore pressure and reduces friction between the grains. This reduction of frictional contact strength decreases the shear strength of soil. The failure plane typically forms at the contact between the two contrasting materials and the overlying material begins to travel downslope (Ellen and Flemming, 1987).

Once failure occurs, the saturated soil moves down-slope in different ways. Some shallow landslides form a slump in which the failed material moves as a single, coherent block or series of coherent blocks (fig. 3; Cruden and Varnes, 1996). These failures slowly travel a short distance, often with vegetation intact on top of the blocks of soil. The failed material frequently remains within or directly down-slope from the scar of the landslide, concealing the failure plane and creating a bulge at the toe of the failure (Ellen and Flemming, 1987).

In contrast to slumps, some shallow landslides mobilize into debris flows in which the failed material liquefies and travels rapidly down-slope, sometimes up to several kilometers (fig. 1; Cruden and Varnes, 1996; Ellen and Flemming, 1987). During a debris flow, the failed material typically completely evacuates the scar, leaving the failure plane exposed (Gabet and Mudd, 2006). The liquefied soil flows down the hillside or follows channelized valleys and can scour the surface, entraining more material into the flow (Ellen and Flemming, 1987, Mckenna et al., 2012). The debris flow continues to travel until it encounters an obstacle in its path or the slope decreases to a point that flow cannot be sustained (Ellen and Flemming, 1987; Stock and Dietrich, 2003). These two contrasting styles of down-slope movement are not mutually exclusive and often the behavior of a shallow landslide shows characteristics of both slumps and debris flows. (Ellen and Flemming, 1987).

2.2 Previous studies

Previously, researchers have hypothesized that failure mode depends on soil bulk density. (e.g., Ellen and Flemming, 1987; Iverson et al., 1997; Iverson et al., 2000, Gabet and Mudd, 2006, Mckenna et al., 2016). In previous studies, laboratory tests have demonstrated that soils with low bulk density are more likely to mobilize into a debris flow during a shallow landslide (Casagrande, 1975; Ellen and Flemming, 1987; Iverson et al., 2000).

Casagrande (1975) observed the behavior of loose and dense soils during deformation using direct shear tests of sand. He found that stresses applied to sand are accommodated by deformation along a failure plane and that during deformation, loose, low bulk density sands behave differently than dense, high bulk density sands (fig. 5). Both sands deform to reach a critical bulk density along the failure plane, but dense sands dilate to reach this critical bulk density while loose sands contract (Casagrande, 1975).

It has been widely hypothesized (Ellen and Flemming, 1987; Iverson et al., 2000, Gabet and Mudd, 2006, Mckenna et al., 2016) that during a shallow landslide, the failed material behaves similarly to the sands in Casagrande's shear tests; that is, during deformation, loose soils contract while dense soils dilate to reach a critical bulk density. During a shallow landslide, however, the soil is saturated. This is believed to be the mechanism responsible for the mobilization of a landslide into a debris flow (Ellen and Flemming, 1987; Flemming et al., 1989; Iverson et al., 1997; Iverson et al., 2000). Given the contrasting behavior of loose and dense soils during deformation, the critical bulk density first proposed by Casagrande (1975) acts as a threshold that separates soils that are likely to mobilize into debris flows from soils that are likely to slump during a shallow landslide.

When a saturated, loose soil contracts, the reduction in pore volume increases the pore pressure between grains. If this reduction of pore space occurs faster than water can drain from the soil, liquefaction occurs (Casagrande 1975; Ellen and Fleming, 1987; Iverson et al., 2000). This causes material to accelerate quickly down slope as a debris flow (Casagrande, 1975; Ellen and Fleming, 1987; Iverson et al., 2000). These flows from loose soils come to rest only when the material encounters an obstacle or becomes too thin to maintain the pore pressures necessary for flow, often at a reduction in slope (Ellen and Flemming, 1987; Stock and Dietrich, 2003).

In saturated, dense soils, the dilation associated with deformation increases volume and decreases pore pressure; liquefaction does not occur. Although debris flows have been observed in dilative soils, they are far less common than in loose soils because they require higher water content to produce the pore pressure necessary for flow (Ellen and Flemming, 1987; Flemming et al., 1989). When debris flow mobilization does occur in dilative soils, it tends to be episodic, slow, or the flow travels only a short distance before deposition (Ellen and Flemming, 1987; Iverson et al., 2000).

In a more recent study, Iverson et al. (2000) simulated landslides in a laboratory flume to test the hypothesis that soils with low bulk densities are more likely to mobilize into a debris flow. Although Iverson's paper is focused on porosity, porosity is derived from bulk density measurements in the study. They measured density, pore pressure, displacement and observed failure mode during failure of an artificial slope of sandy loam soil (fig. 6). As expected, loose soil (bulk density < 1.30 g/cm^3) contracted, giving rise to elevated pore pressure and rapid flow of material down slope. In dense soil (bulk density > 1.59 g/cm^3), motion was slow and episodic or they were not able to induce landsliding at all. With medium density soil (bulk density between 1.30 g/cm^3 and 1.59 g/cm^3) the results were inconsistent, with a mix of contractive and dilative behaviors.

While laboratory experiments have established the differences in behavior between high and low density soils, field studies have produced mixed results. Gabet and Mudd (2006) compared porosity (derived from bulk density measurements) at eight shallow landslide sites in the Sedgwick Reserve, near Santa Barbara, CA. They sampled soils at four debris flow sites and four slump sites and found no statistically significant difference in density between the soils at the two types of failures. In addition, triaxial tests produced unexpected results: both the soils from the slump sites and debris flow sites dilated during shear deformation. Gabet and Mudd (2006) proposed that dense soils can initially dilate beyond the critical density, then contract during a subsequent episode of deformation, thus initiating a debris flow (Flemming et al., 1989).

In a larger study, Mckenna et al. (2012) sampled soils at 96 shallow failures in western Oregon and southeast Colorado. They calculated the predictability of failure mode using seven variables: slope, volume, geomorphic setting, Approximate Mobility Index, bulk density, percent fines and saturated conductivity. In addition, they added measurements from Gabet and Mudd (2006) and flume data from Iverson et al. (2000) to their analysis. They concluded that the most accurate predictor of failure mode is a combination of percent fines (silt and clay passing through a #200 sieve) and soil bulk density. They concluded that percent fines changes the critical density between dilative and contractive soils and they developed an equation to predict failure mode within their data set with 79% accuracy (Mckenna et al., 2012).

This approach is problematic, however, because of the combination of data sets and sampling techniques. The study relies heavily on Gabet and Mudd (2006) for soils with high fine-grained content and depends on Iverson's (2000) flume data for dense soil (> 1.6 g/cm^3) measurements. Furthermore, Mckenna et al. (2012), Gabet and Mudd (2006) and Iverson et al. (2000) used three different sampling techniques (core method, resin-coated clod technique and excavation method, respectively) that are known to yield values inconsistent to each other (Page-Dumroese et al., 1999).

Considering the issues with conventional bulk density measurement techniques, the combination of data sets and sampling techniques leave room for uncertainty in conclusions from Mckenna et al. (2016). A skeptic could make the case that the hypothesized critical bulk density changes with percent fines is an artifact created by the inconsistencies between sampling techniques.

Another issue is that Mckenna et al. (2016) did not consider the experimental error involved when testing for seven variables. When testing multiple variables, the probability of producing a false positive result increases exponentially. In each of the F and T tests performed in the study, the threshold for statistical significance, α, is set at 0.05, which is appropriate for testing only one variable. When testing seven variables with α set at 0.05 for each variable, the chance of producing at least one false positive result among the seven variables is 30%. Typically, the "experiment-wise" risk of a false positive for all variables considered together should be under 5% for a positive finding to be considered significant.

The challenges with these studies based on conventional bulk density sampling techniques highlight an opportunity to use new technology to test the same hypothesis more accurately and precisely.

In this study I tried to improve on previous work by

1) Focusing on one variable (bulk density) to avoid the issues of producing a false positive result when testing multiple variables
2) Using one method of bulk density measurement performed exclusively in the field to avoid the issues of combining data sets and inconsistencies between measurement techniques
3) Employing a more thorough field sampling protocol (discussed in the methods and discussion section) to produce a more representative average bulk density for soil at a given landslide
4) Use of a more accurate and precise tool

These methods and the new tool allowed me to estimate the values for critical bulk density that separate soils that slumped from soils that mobilized into debris flows during historic storms. Additionally, I tested whether soils with low bulk density produce landslides with longer debris flow runouts. I also measured how bulk density changes laterally at different sites around a scarp and how bulk density changes with depth vertically through the soil column.

3.0 METHODS

To accurately characterize the density of soils at shallow landslide sites I selected landslide scars throughout Marin County (fig. 1) and used the MILT to perform bulk density measurements. I used aerial imagery in Google Earth and a USGS digital map of landslides from 1982 and 2006 (Stock, unpublished) to choose sample sites. At each site, I recorded landslide geometry, soil properties, collected soil samples and used MILT to make 3D scans of the soil surface. In the lab, I dried and weighed the soil samples, and estimated the density by dividing dry mass by excavated hole volumes measured by repeat MILT scans.

3.1 Site Selection and Interpretation

I chose Marin County as my field area because it has numerous shallow landslide scars mapped by Stock. I selected 15 landslide scars to sample: 14 in Marin and one in San Francisco (fig. 1; table 1). Of these 15 scars, I interpreted 11 that mobilized into debris flows, three that failed as slumps and one that mobilized as a debris flow, followed by subsequent slumping.

To locate the debris flows I used an unpublished USGS landslide map developed by Dr. Stock in combination with aerial imagery in Google Earth. The map shows the head scarp, lateral scarps and runout of 1,717 shallow landslides that occurred in Marin County during winter 2006.

Stock's map shows headscarps, lateralscarps and displaced masses. Landslides that mobilized into debris flows have long displaced mass polygons, extending more than ten meters or so from the lateral scarp terminus. In the field, I confirmed the failure mode of the landslide scars; I interpreted scars with the failure plane completely exposed, with no sign of the failed material, to have failed as debris flows. Those that failed as slumps still had material just downslope of head- and lateral scarps.

To locate and identify slumps I used aerial imagery from Google Earth, reports from Stock (SF and I-280 examples) and field observations. I was unable to find any slumps using Stock's 2006 landslide map. I identified slumps by the presence of failed material still within the scar or deposited directly downslope from the scar. In aerial imagery, the scar formed a concave-up topography while the failed material formed a hummocky, convex-up deposit within or downslope from the scar. In the field I confirmed these observations and also interpreted multiple head scarps within the failed material as evidence that the material failed in coherent blocks.

I interpreted one landslide as a hybrid slide because it failed initially as a debris flow then subsequently failed as a slump. The upslope portion of the scar near the head scarp has evidence of a debris flow. There is no evidence of failed material within this portion of the scar and rills had formed in the soil on the floor of the scar. I interpreted this surface as the failure plane. Farther downslope, a second, smaller scarp cuts across the failure plane with a block of failed material offset slightly downward. Farther down slope, the surface is hummocky with several small scarps separating offset blocks of soil. I interpreted this as slumping of the soil that formed the failure plane of the initial debris flow. I interpreted this slumping to have occurred after the debris flow based on the cross-cutting relationship between the slump's head scarp and the debris flow's failure plane.

3.2 Field Procedures

At each landslide scar, I chose a site on or near the headscarp to make a stratigraphic column, collect soil samples and take a series of measurements with the MILT. The soil samples MILT scans were ultimately used to calculate the bulk density of the soil with depth.

I chose a site at the headscarp or the up-slope portion of the lateral scarp to make the stratigraphic column and take bulk density measurements. I chose the site based on the condition of the scarp; I preferred linear, vertical scarps free of vegetation for sampling. At each site I removed the outermost vertical surface of soil from the scarp to expose the layers, record the soil stratigraphy and measure the distance from the soil surface to the failure plane. I used this data to form a stratigraphic column. I took bulk density measurements using the MILT from the same location. Starting from the surface, I took a series of bulk density measurements working incrementally downward until I reached the failure plane. I aimed for 10 measurements between the surface and the failure plane, evenly spaced about 0.1 to 0.2 m apart, depending on the depth of the scar. I based this incremental sampling protocol on the detailed sampling I performed at BRR-02 and WH-02, as described in detail below. In the results section I discuss how this sampling protocol captures a representative sample for the landslide.

Bulk density measurements with MILT require two 3D scans to determine excavated soil volume and a small soil sample to determine mass. First I created a flat, horizontal surface in soil I intended to sample and cleared away any disturbed soil or plant debris. In addition, I trimmed and removed any plant roots protruding from the soil that would create shadows during the MILT scans. With the soil surface cleared, I placed the MILT platform on the soil surface.

The MILT platform was designed with four spikes on the underside that anchor it to the soil surface, preventing it from shifting between scans (fig. 7). It also has a small window through which the MILT's lasers access and image the soil surface. I placed the MILT on the platform and took an initial scan of the soil surface. I then removed the MILT and carefully excavated a small hole in the soil through the window in the platform. I transferred the displaced soil to a heat-resistant sample tin to be oven-dried and weighed. I was careful to transfer any disturbed soil from the hole to the tin to ensure the accuracy of the measurements. Lost soil would be a major source of error in this technique. Additionally, I left a portion of the soil surface surrounding the hole undisturbed for point-cloud alignment later. After I collected the soil sample, I placed the MILT on the platform for a final scan of the soil surface, this time with the soil sample removed.

My sampling was occasionally limited by the presence of cobbles or the battery life of my equipment. Some of the landslides scarps I sampled have sections of soil that are clast-supported, predominantly by cobbles. This made it difficult, and in some cases impossible, to drive the spikes of the MILT platform into the soil surface and to excavate soil. In these cases, I was unable to perform measurements on the sections of the scarp with the cobbles. Also, occasionally my laptop batteries would be depleted before I completed sampling the full vertical section of the scarp. These problems prevented me from performing the full 10 measurements at some of the slides.

3.3 Lab Procedures

After fieldwork, I processed the MILT scans and soil samples. I used the two MILT scans taken in the field to calculate the volume of the soil samples taken from the landslide scarps and then weighed them to determine their mass. The mass of the soil sample divided by its volume equals the bulk density of the sample.

I used CloudCompare 2.6.1 to process the 3D scans produced by the MILT and determine the volume of the soil sample. Each scan was converted to a point cloud as it was imported to CloudCompare (fig. 8). I loaded the initial and final scans for a given sample and aligned the scans using the undisturbed soil surface surrounding the hole. I then calculated the volume between the two clouds using the tools built into CloudCompare. A more detailed description of the CloudCompare procedure is included in Appendix 1.

I determined the mass of each soil sample by oven-drying the samples to drive off moisture and then weighing the soil sample. I baked each sample for 24 hours at 105° and then weighed them on a Ohaus E4000D scale accurate to 0.01 grams. I then returned the samples to the oven for another 24 hours of baking. I weighed the soil once more to ensure that all the water had been driven from the soil.

3.4 Wax Trials

I assisted Jonathan Stock with his evaluation of the precision of the bulk density measurements produced using the MILT. He employed the method described above, using the MILT to measure the density of blocks of paraffin wax, which have a uniform density. He performed 20 measurements on two blocks of wax and found that for each block of wax, all measurements were within 2% of each other. This 2% uncertainty applies to all bulk density values reported in this study and accounts for the precision of the MILT and scale and any error due to excavated wax spilled or missing when determining mass.

3.5 Detailed Sampling

At the beginning of my field work, I performed detailed bulk density sampling at two landslide scars to characterize the spatial variability of bulk density around a landslide scarp. I used this data set to develop a sampling protocol that captures a representative average density. I used this protocol for the rest of the slides I sampled. In this section I outline the field process of the detailed sampling. The results of the detailed sampling and the justification of the sampling method I developed are covered in the results section.

I chose Big Rock Ridge Slide 2 (BRR-02) and White Hill Slide 2 (WH-02), shown in Figure 9, for detailed sampling. These soils had contrasting characteristics: WH-02 had distinct layering while BRR-02 did not. At BRR-02 I took 39 bulk density measurements from 5 sites, evenly spaced around the scarp of the scar (fig. 10). At each site I took measurements incrementally from the surface to the failure plane. By using this incremental approach, I captured the vertical variability in bulk density with depth through the soil column. By performing these incremental measurements at five sites around the scar, I captured the lateral variability in bulk density around the scar.

At WH-02 I made 30 bulk density measurements at a site on the up-slope section of the west lateral scarp (fig. 11). The goal of this sampling was to capture the variability of soil bulk density with depth in layered soils. I used the same incremental approach, starting at the surface and working incrementally downward through the soil column to a depth of 1.57 m. The failure plane was at a depth of 2.10 m but I was unable to reach it for sampling; the gradual curve of the scarp from vertical to horizontal would have required too much excavation to reach the failure plane.

4.0 RESULTS

I used my field data and statistical analysis to test the hypothesis that slumps occur in higher density soils than landslides that mobilized into debris flows. The following sections provide an overview of my bulk density measurements, the statistical tests I used, and a summary of the data I produced from the detailed sampling I performed on two landslide scars.

4.1 Field Data

For my analysis I used 178 bulk density measurements from soils at 15 shallow landslide scars, primarily in Marin County, and one from Twin Peaks, San Francisco (fig. 1; Table 1). Of the 15 slides, I interpreted 11 to have mobilized into debris flows, three to have failed as a slump and one as a hybrid failure. The bulk density measurements range from 0.727 g/cm^3 to 1.96 g/cm^3 and have 2% uncertainty. The runout lengths of the landslides range from 12 m to 375 m, determined from Stock's mapping and aerial imagery. A table of all data is in Appendix 2.

Figure 12 shows all 178 bulk density measurements plotted as a function of depth. There is considerable scatter in the data but generally the deeper measurements are denser. Although there is considerable overlap, the measurements from the slump sites are clustered toward the high-density side of the plot.

Figure 12 also illustrates that over 98% of the measurements from debris flow sites fall under a threshold of 1.62 g/cm^3, regardless of depth below surface. The measurements from slump sites, on the other hand, have an upper threshold of about 1.83 g/cm^3, but this upper threshold is only reached by the deeper measurements (depth greater than 0.8 m below surface).

I excluded 19 bulk density measurements from my analysis because of poor quality, missing data or because the landslide was a bedrock failure instead of a soil failure, which is not the focus of this study. I made the decision to exclude data while in the field, before calculating the bulk density to avoid bias. Also, while learning to use the MILT, I performed 20 trial bulk density measurements at several landslide sites. These measurements were not taken incrementally between the soil surface and the failure plane as were the measurements from the majority of the landslides. I excluded these measurements to maintain a consistent sampling protocol for the data I used in my analysis. These 39 excluded measurements are included in Appendix 3.

4.2 Statistical Analysis

I tested my hypothesis three ways. First, I used a T-test to compare the average of all the bulk density measurements from soil at debris flow sites to the average of all the measurements from soil at slump sites. I also calculated a slide-average density for the soil at each landslide and used a T-test to compare the slide-average bulk density from soil at debris flow sites to the slide-average bulk density of soil at slump sites. Finally, I used linear regression to test for an effect of soil bulk density on landslide runout length.

The purpose of my first test was to establish a difference in the average density between the soil from debris flow sites and the soil from slump sites. In figure 12, the slump sites appear to have a higher average density than the debris flow sites. To establish that this trend in density is significant, I used a two tailed T-test (fig. 13). For this analysis I used 152 bulk density measurements: 124 from soil at debris flow sites and 28 from soil at slump sites. The T-test confirms (Prob > |t|=0.0001) that the average density measurements of the soil at debris flow sites (1.361 +/- 0.016 g/cm^3; mean +/- S.E.) is significantly lower than the average density of the measurements from the soil at slump sites (1.591 +/- 0.029 g/cm^3; mean +/- S.E.). All plus/minus values represent the standard error of the mean.

For my second test, I calculated the average soil density for each slide, then compared the average of debris flow slide-averages to the average of the slump slide-averages (fig. 14). For this analysis I used data from 11 debris flows and 3 slumps. Again, I used a two tailed T-test to compare the averages of these two populations. The T-test confirms (Prob > |t|=0.0002) that the average density of soil at debris flow sites (1.341 +/- 0.046 g/cm^3; mean +/- S.E.) is significantly lower than the average density of soil from slumps sites (1.604 +/-0.016 g/cm^3; mean +/- S.E.).

The T-test using the slide-averages is the strongest indicator that mobilized landslides occur preferentially in low density soils (fig. 14). When comparing the average densities of soils at debris flow sites to the average densities of soils at slump sites, there is no overlap in the data; the debris flow site with the highest slide-average soil density (1.48 g/cm^3) has a lower density than the soil from the slump with the lowest slide-average soil density (1.57 g/cm^3). This suggests that the critical bulk density, a concept first introduced by Cassagrande (1975), lies between 1.48 g/cm^3 and 1.57 g/cm^3.

For both of these T-tests I excluded 26 surface measurements because they were problematic during analysis. These measurements are colored grey in figure 12. At each landslide I took a measurement as close as possible to the soil surface for my initial measurement before working incrementally downward. These 26 measurements were from the top 0.1 m of soil and have a noticeably lower density than the rest of the population. These low density surface measurements added considerable scatter to the overall population of density measurements and were systematically less dense that the bulk of the failed material. More importantly, with these surface measurements included, they created a bias when calculating the average mean density for a given landslide scar; a scar with fewer measurements would be more dramatically affected by a low-density surface measurement. This would result in a falsely low average bulk density compared to a scar with more measurements. To avoid these complications during analysis, I excluded these measurements.

My final test compared the landslide runout length to the slide-average soil bulk density for each site (fig. 15). For this analysis I used the slide-average soil density from 14 landslide sites: 10 debris flows, 4 slumps and the hybrid, debris flow/slump. Linear regression revealed that bulk density has no significant effect on mapped runout length.

The linear regression of landslide runout and bulk density demonstrated that bulk density is a poor predictor of landslide runout (fig. 15). This is likely due to the the effect of numerous other factors that control debris flow deposition. These might include obstacles, breaks in slope, sharp turns in a channel the debris flow is following, or where the channel itself terminates and becomes open slope or flat ground (Ellen and Flemming, 1987; Stock and Dietrich, 2003).

4.3 Detailed Sampling

I performed detailed sampling on two landslide scars: Big Rock Ridge Slide 2 and White Hill Slide 2 (fig. 9). Both of these failures mobilized into debris flows but had contrasting soil characteristics; the White Hill slide had distinct layering while the Big Rock Ridge slide did not. The goal of this detailed sampling was to characterize the spatial variability of bulk density around a given landslide scar to develop a sampling technique that captured a representative average density for the entire landslide.

At Big Rock Ridge Slide 2 (BRR-02) I took 39 bulk density measurements from 5 sites, evenly spaced around the scarp of the scar (fig. 10). At each site I took measurements incrementally from the surface to the failure plane. Figure 16 shows a photo of one of the columns of soil (site 3), a stratigraphic column displaying the soil characteristics and a plot of bulk density vs. depth displaying the measurements from all 5 sites on the slide. The photo, stratigraphic column and density plot are scaled and aligned so the depth matches on all three.

The soil at BRR-02 is a mixture of pebbles floating in a sandy silt matrix (fig. 16). Soil is roughly 0.75 m deep, over sandstone bedrock. This bedrock forms the failure plane of the debris flow. Aside from the bedrock and a thin, upper root-rich layer, the soil shows no signs of stratification or horizon development. There are signs of bioturbation such as small holes interpreted as burrows which may be responsible for the heterogeneity and lack of stratification/horizon development.

The bulk density measurements from this slide range from 0.789 g/cm^3 to 1.96 g/cm^3 and show considerable scatter (fig. 16). As with the soil at most of the slides, the lowest soil density occurs at the surface. Aside from the low surface measurements and one anomalously high measurement, the density of the majority of the material falls between 1.35 g/cm^3 and 1.60 g/cm^3 and shows no sign of increased density with depth.

The scatter in bulk density is due to density variability in the soil, not inter-site variability. Figure 17 shows that the average density for sites on the up-slope end of the scar (sites 1-3) is similar to the average density of the scar overall. The average density for the two sites on the down-slope end of the scar are farther from the overall average density. Although there are differences in the mean density of each individual site, ANOVA analysis (Fig. 17) confirms that the scatter in the population is not due to this grouping (Prob>F = 0.4291).

For this analysis (including calculating slide and site average densities), I excluded the surface measurements and the one anomalously high point. I also excluded surface measurements because they comprise a small part of the mass of the slide, and have considerable scatter that biases average density. I treated an anomalously high point as an outlier and excluded it because it was more than 3 standard deviations away from the mean density.

I also made detailed measurements at White Hill Slide 2 (WH-02). Here I made 30 bulk density measurements at a site on the up-slope section of the west lateral scarp (fig 11). This debris flow scar is 2.1 m deep and bedrock is not exposed within the scar. The floor of the scar is a planar soil surface with rill development. I interpreted this planar section as the failure plane with rills formed from overland flow through the scar.

In contrast to BRR-02, the soil at the scar of WH-02 has signs of stratification and horizon development (fig. 18). From the surface to 0.8 m depth there is a mixture of pebbles, sand and silt, with a gradual fining with depth. Roots gradually diminish and the soil shows increased signs of weathering—for example, color change, increased cohesion and changes from blocky peds to massive structure. In addition, gravel clasts are weathered to clay locally. At 0.8 m depth there is a sharp contact with a different underlying material. Like the soil above, it is a mixture of sand, silt and pebbles, but with the exception of a thin, gravel-rich layer at 1.33 m, the pebble content overall is notably less. This layer has a darker color and is more uniform and cohesive. It extends down to at least 1.77 m, where I stopped digging.

The soil at WH-02 showed an increase of bulk density with depth (fig. 18). The most dramatic change in density occurs at the sharp contact at 0.8 m, probably due to a change in material with a higher fine-grained content below the contact. These finer grains fill the void spaces between the sand and pebble grains, increasing soil density. I interpreted this layer to have higher fine-grained content based on the uniformity and cohesiveness of the soil. The thin, gravel-rich layer at 1.32 m has the highest density at 1.50 g/cm^3. This is likely because gravel creates pockets of high density that increase the overall density for the layer.

The top layer of soil at WH-02 produced some high density measurements which were unexpected because they are similar to densities in the rest of the slide (fig. 18). In almost every other slide the surface measurements (less than 0.1 m depth) are notably lower than the rest of the population. The high density in WH-02 is likely due to an error made during sampling. I sampled this slide over the course of several days and took surface measurements where I had previously entered and exited the scar. This activity likely compacted the surface causing the density to increase from 0.874 g/cm^3 to 1.15 g/cm^3 between measurements.

The detailed sampling at BRR-02 and WH-02 demonstrates a relationship between soil layering and density changes with depth. I observed this relationship at most of the scars I sampled. Scars like BRR-02 that lacked stratification or clearly-visible soil horizons did not show a trend in bulk density with depth and many had considerable variability (fig. 16). Landslide scars like WH-02 with clear stratification or soil horizons showed an increase in bulk density with depth at layer boundaries (fig. 18). Within a single layer, however, there is no systematic increase of density with depth.

The detailed sampling I performed at BRR-02 and WH-02 was the basis for the sampling technique I used for the rest of the landslides. Of the 5 sites I sampled at BRR-02, the soil at sites at the up-slope end of the scar near the head scarp were closest to the mean soil density of the scar overall (fig. 17). For this reason, I chose sites on the up-slope end of the scar for the rest of landslides I sampled. WH-02 showed an increase of density with depth and for this reason I spaced my measurements incrementally between the surface and the failure plane to capture the full range of densities (fig. 18). This sampling technique produces a more representative sample than the common protocol of taking a single bulk density measurement halfway between the surface and the failure plane.

My approach to sampling was employed most successfully on landslides that mobilized into debris flows. Compared to the slumps, these had well-formed vertical scarps and the failure plane was well-exposed. This allowed full access to the soil column from the surface to the failure plane, with minimal excavation. At most of the slumps, on the other hand, the failed material remained in the scar and concealed the failure plane. This created several problems. First, it was unclear how to space my measurements when the depth of the failure plane was unknown. Second, it was difficult to take measurements at depth without a considerable amount of excavation. On some slumps this made the failure plane, which was at depth under the slumped material, nearly impossible to reach or identify. At the slump in Twin Peaks, the scarp was well formed and the failure plane exposed, but the material too consolidated to dig more than about halfway to the failure plane. These issues with sampling slumps likely resulted in lower density averages for these features because these features showed stratification/horizon development and an increase of density with depth. More accurate sampling would likely strengthen my results, however, by increasing the average density of the slumps.

5.0 DISCUSSION

This study shows that shallow landslides that mobilized as debris flows have soil bulk densities that are measurably less than those that failed as slumps. The transition between those two styles of failure, roughly 1.5-1.6 g/cm3, is consistent with the results of Iverson et al.'s (2000) laboratory flume studies. By using this critical bulk density and the incremental method of bulk density sampling, researchers could identify hillslopes prone to debris flows more accurately than using conventional methods of bulk density measurement.

5.1 Comparison with Previous Studies

The results of my study are consistent with previous studies (Cassagrande, 1975; Ellen and Flemming, 1987; Iverson et al., 1997; Iverson et al., 2000, Gabet and Mudd, 2006, Mckenna et al., 2016) that have suggested loose soils are more likely to mobilize into debris flows. Because my study was exclusively done in the field, it adds merit to the results of previous studies performed in laboratory settings such as Iverson et al. (2000). Both my study and the Iverson et al. (2000) study have found soil density to be a key factor in debris flow mobilization and constrain the values for the critical bulk density proposed by Casagrande (1975; fig. 5).

Iverson et al. (2000) found that soils with densities below 1.30 g/cm^3 mobilize into debris flows while soils with densities above 1.59 g/cm^3 mobilize into slumps. Soils in between, with bulk densities between 1.30 g/cm^3 and 1.59 g/cm^3, had characteristics of both debris flows and slumps during failure. This is a strong indicator that these failures were near the critical bulk density. These density values (1.30 g/cm^3 to 1.59 g/cm^3) bracket the range I found for critical bulk density, which is 1.48 g/cm^3 and 1.57 g/cm^3. The low end of my range is considerably higher, but the upper limits are nearly identical.

There are several possible reasons for the difference in the values for critical bulk density between my study and Iverson et al. (2000). In the Iverson (2000) study, researchers placed a prism of soil behind a wall at the top of the flume and compacted it using foot traffic or mechanical vibrations to simulate a stable hillslope. These unnatural mechanisms for deposition and compaction are different from the mechanisms that compacted the soils at my field sites. In a natural setting, solid bedrock weathers during soil formation and becomes less dense over time. Slow, downslope transport of soil affects the density of the soil and the arrangement of the grains. These different mechanisms that occur in the flume and on a natural hillslope could affect the packing of grains and cause a difference in the critical bulk density.

The different bulk density sampling methods could also account for the differences in critical bulk density values between my study and Iverson et al (2000). Both our studies used an excavation method, but Iverson et al. (2000) used a conventional method for measuring soil volume that employs either a sand cone or rubber balloon (described in Blake, 1965). My study used the MILT to determine soil volume and it is possible that the two methods produce different results.

Similarly, the combination of data sets and different techniques for measuring bulk density in McKenna et al. (2012) make comparison challenging. Since different methods of bulk density measurement produce inconsistent values, any conclusions drawn about similarities or differences in our results may be an artifact of sampling inconsistencies. In addition, without grain-size analysis it is difficult to compare my results to Mckenna et al. (2012), who found that the critical bulk density can range from 1.04 g/cm^3 to approximately 1.65 g/cm^3, depending on the percentage of fine grains. Although my values for critical bulk density fall within this range, the majority of all my data also fall within this range. However, the upper limit of 1.65 g/cm^3 for critical bulk density in Mckenna and others (2012) is similar to my finding of 1.57 g/cm^3.

5.2 Hillslope Safety, Critical Bulk Density and Sampling Protocol

Given the destructive nature of debris flows compared to slumps, locating slopes susceptible to debris flows would help identify safe places for building and would improve public safety. This study indicates that bulk density could be used as a tool for predicting debris flow prone slopes. Steep slopes with soils below the critical bulk density should be labeled as hazardous because they are prone to debris flows during heavy rainfall. Steep slopes with soils above the critical bulk density would be more likely to slump and could be labeled less hazardous.

This study, like previous studies, offers a range of values for critical bulk density (1.48 g/cm^3 and 1.57 g/cm^3). Although the lower limits of the range differ between the studies, the upper limits of the range are similar between this study

(1.57 g/cm^3), Iverson et al., (2000) (1.59 g/cm^3) and Mckenna et al., (2012) (1.65 g/cm^3). Furthermore, figure 12 shows that 98% of bulk density measurements from soil at debris flow sites fall below the threshold of 1.62 g/cm^3. Because these studies offer a range of possible values for critical bulk density, a cautious approach would be to use the highest upper limit of the range (e.g. 1.65 g/cm^3), plus a factor of safety, to evaluate soil on hillslopes. This would reduce the risk of labeling a potentially debris flow-prone slope as safe.

This study also illustrates that the conventional methods of bulk density measurement on landslides would be insufficient for evaluating hillslope safety. The common protocol of using one bulk density measurement to represent the density of the entire failed material risks mischaracterizing the material's overall density. The hybrid slide was an example of a slide that would be incorrectly labeled as safe from debris flows. In this slide, the low density top layer, which was less than 0.75 m thick, mobilized into a debris flow. The underlying high density layer extends to a depth of at least 1.55 m and formed a slump. The density of this layer ranges from 1.45 to 1.83 g/cm^3. Because the slumped material remained in the scar, I was unable to reach the failure plane, which is likely even deeper than 1.55 m. A single measurement taken half way to the potential bedrock failure plane would measure the density of the dense lower layer and incorrectly characterize the soil density as greater than the critical density necessary for debris flow mobilization. This would produce a false conclusion of safety from debris flows on a potentially hazardous slope.

The risk of mislabeling a hillslope as safe can be decreased by performing a more detailed series of bulk density measurements, similar to the methods used in this study. Starting at the soil surface and taking measurements incrementally to the bedrock gives a more complete picture of the density changes in the soil column which may have complex variation in density with depth. This method would produce a more representative mean density for the material and give a more accurate prediction of its debris flow potential if it failed. However, even a representative mean density is an oversimplified evaluation for debris flow potential. For example, soils with a low density top layer and a dramatically denser bottom layer (like the soil in the hybrid slide) could have a mean density above the critical bulk density and the hillslope would be labeled as safe from failing as a debris flow. This overlooks the potential for the top layer, which could be lower than critical density, to fail as a debris flow.

With more complex analysis, the incremental method has the potential to identify debris flow hazards that calculating a mean density would miss. In the above scenario, a plot of bulk density vs. depth would highlight the low density of the material in the top layer and its potential for failing as a debris flow. The plot would also highlight the dramatic change in density that would likely be associated with a change in permeability. This contrast in permeability between the two layers would be identified as a location where ponding would occur during heavy rainfall, which is a precursor to a debris flow. A researcher could evaluate the density vs. depth plot and identify the location of the dramatic change in density as a probable failure plane of a debris flow.

Another possible method of evaluating debris flow potential would involve careful evaluation of the soil stratification before beginning bulk density measurements. The detailed sampling at WH-02 revealed that increases in bulk density occurred over sharp contacts between layers. Since there was no systematic increase in soil density within layers, researchers could calculate an average density for each layer. This could eliminate the time-consuming process of incremental excavation and measurement while still identifying individual layers prone to fail as a debris flow that would be overlooked by the conventional protocol.

6.0 CONCLUSION

I used the MILT, a portable 3D scanner developed by NASA and USGS, to measure the bulk density of soils adjacent to landslide scars in Marin County. Using this new field method of bulk density measurement, I tested the hypothesis that soils that fail as slumps are measurably denser than those that mobilize into debris flows. I also examined the spatial variability of bulk density around a landslide scar and used the results to develop a sampling protocol that produces a more representative average density than convention sampling protocols for the soil around a landslide.

My results indicate that soils that fail as slumps are measurably denser than those that mobilize into debris flows. The most likely explanation is that loose soils contract, increasing pore pressure and leading to liquefaction and debris flows. The dilation of high bulk density soil inhibits movement and causes a slump to occur. For the 15 scars I sampled, the average of slide-average densities for soil at debris flow sites (1.34 +/- 0.043 g/cm^3; mean +/- S.E.) is lower than the average of slide-average densities for soil at slump sites (1.60 +/-0.081 g/cm^3; mean +/- S.E.). The absence of overlap in the slide-average densities between debris flows and slumps indicates that the critical bulk density is between 1.48 g/cm^3 and 1.57 g/cm^3.

The detailed sampling I performed at two landslides demonstrates different ways bulk density changes with depth. Soils with layering (stratification or soil horizons) show a marked increase in density with depth. The increase in density is most dramatic over sharp contacts between layers and transitions to gravel-rich layers. Within individual layers there is no systematic increase in density. Soils that lack layering do not show an increase in density with depth. These soils have randomly scattered densities and signs of bioturbation.

Given the variable nature of soil density, a thorough method of measuring density is necessary to successfully evaluate hillslope safety from debris flows. The common protocol of using one measurement to represent the entire failed material can miss potential hazards in soils with density that changes dramatically with depth. By taking incremental measurements from the soil surface to the bedrock, or careful evaluation and sampling of individual soil layers, researchers can identify sharp increases in density as likely failure planes for future debris flows.

7.0 REFERENCES

Benites, V.M., Machado, P.L.O.A., Fidalgo, E.C.C., Coelho M. R., and Madari, B. E., 2007, Pedotransfer functions for estimating soil bulk density from existing soil survey reports in Brazil: Geoderma, v. 139, p. 90–97

Blake, G.R., 1965, Methods of Soil Analysis (C. A. Black, D. D. Evans, J. L. White, L. E. Ensminger, & P. E. Clark, Eds.): American Society of Agronomy, Madison, WI, p. 374-390

Casagrande, A., 1975, Liquefaction and cyclic deformation of sands; a critical review: Memorias del Congreso Panamericano de Mecanica de Suelos e Ingenieria de Fundaciones in Proceedings of the Panamerican Conference on Soil Mechanics and Foundation Engineering, p. 79–133.

Cruden, D.M., and Varnes, D.J., 1996, Landslides: investigation and mitigation. Chapter 3-Landslide types and processes: Transportation research board special report 247, p. 36-75

Duncan, J.M., 1996, Landslides: investigation and mitigation. Chapter 13-Soil Slope Stability Analysis: Transportation research board special report 247, p. 337-371

Ellen, S.D., and Fleming, R.W., 1987, Mobilization of debris flows from soil slips, San Francisco Bay region, California: Reviews in Engineering Geology, v. 7, p. 31–40.

Ellen, S. D. and Wieczorek, G. F., eds., 1988, Landslides, floods, and marine effects of the storm of January 3-5, 1982, in the San Francisco Bay region. U. S. Geological Survey Professiona Paper 1434: 310 p.

Fleming, R.W., Ellen, S.D., and Algus, M.A., 1989, Transformation of dilative and contractive landslide debris into debris flows; an example from Marin County, California: Engineering Geology, v. 27, p. 201–223.

Grove, K., Colson, K., Binkin, M., Dull, R., and Garrison, C., 1995, Stratigraphy and structure of the Late Pleistocene Olema Creek Formation, San Andreas fault zone north of San Francisco, California, in Sangines, E., Andersen, D., Buising, A., eds., Recent Geologic Studies in the San Francisco Bay Area: Society for Sedimentary Geology (SEPM) Pacific Section Book 76, p. 55-77.

Gabet, E.J., and Mudd, S.M., 2006, The mobilization of debris flows from shallow landslides: Geomorphology, v. 74, p. 207–218.

Heuscher, S.A., Brandt, C.C., and Jardine, P.M., 2005, Using soil physical and chemical properties to estimate bulk density: Soil Science Society of America Journal, v. 69, p. 51–56.

Iverson, R.M., Reid, M.E., and LaHusen, R.G., 1997, Debris-Flow Mobilization from Landslides: Annual Review of Earth and Planetary Sciences, v. 25, p. 85–138, doi: 10.1146/annurev.earth.25.1.85.

Iverson, R.M., Reid, M.E., Iverson, N.R., LaHusen, R.G., Logan, M., Mann, J.E., and Brien, D.L., 2000, Acute sensitivity of landslide rates to initial soil porosity: Science, v. 290, p. 513–516.

Lavelle, J. P., Schuet, S. R., and Derouen, M., 2007, A Handheld, wireless 3D laser scanner for shuttle tile inspection: Buenos Aires, 1-6.

McKenna, J.P., Santi, P.M., Amblard, X., and Negri, J., 2012, Effects of soil-engineering properties on the failure mode of shallow landslides: Landslides, v. 9, p. 215–228.

Miller, R.E., Hazard, J., and Howes, S., 2001, Precision, accuracy, and efficiency of four tools for measuring soil bulk density or strength: United States Department of Agriculture General Technical Report PNW-RP-532, April 2001

Montgomery, D.R., Dietrich, W.E., 1994. A physically based model for the topographic control on shallow landsliding. Water Resources Research 30, 1153–1171.

Nilsen, T.H., 1979, Relative slope stability and land-use planning in the San Francisco Bay region, California: U.S. Govt. Print. Off., 110 p.

Page-Dumroese, D.S., Brown, R.E., Jurgensen, M.F., and Mroz, G.D., 1999, Comparison of methods for determining bulk densities of rocky forest soils: Soil Science Society of America Journal, v. 63, p. 379–383.

Stock, J., Dietrich, W. E., 2003, Valley incision by debris flows: Evidence of a topographic signature: Water Resources Research, v. 39, no. 4, 1089

Wilson, C.J., Dietrich, W.E., Peven, D.A., and Anonymous, 1986, The contribution of shallow groundwater flow in bedrock to storm runoff and high pore pressure development in hollows: Eos, Transactions, American Geophysical Union, v. 67, p. 957.

8.0 TABLES

Table 1: Summary of data from the 15 landslides used for analysis.

Landslide	Debris Flow or Slump	Average Bulk Density Without Surface (g/cm3)	runout (m)	Bedrock	Number of Samples	Standard deviation	Standard Error	Lat/Long
Big Rock Ridge Slide 1	Debris Flow	1.46	30	sandstone	11	0.080	0.024	38.040790°, -122.570869°
Big Rock Ridge Slide 2	Debris Flow	1.47	375	sandstone	36	0.126	0.021	38.035335°, -122.554678°
Big Rock Ridge Slide 3	Debris Flow	1.45	69	sandstone	5	0.106	0.047	38.035248°, -122.564971°
White Hill Slide 1	Debris Flow	1.06	33	volcanic	5	0.144	0.064	37.991647°, -122.631663°
White Hill Slide 2	Debris Flow	1.23	172	volcanic	25	0.140	0.028	37.995334°, -122.629065°
White Hill Slide 3	Debris Flow	1.17	29	volcanic	7	0.135	0.051	37.993023°, -122.624838°
Walker Creek Ranch Slide 1	Debris Flow	1.44	104	sandstone	6	0.094	0.039	38.185631°, -122.818787°
Walker Creek Ranch Slide 2	Debris Flow	1.47	27	sandstone	8	0.111	0.039	38.183688°, -122.817223°
Walker Creek Ranch Slide 3	Debris Flow	1.36	226	sandstone	7	0.162	0.061	38.183661°, -122.825834°
Point Reyes Slide 1	Debris Flow	1.18	79	granite	6	0.135	0.055	38.078123°, -122.861310°
Mount Tamalpais Slide 1	Debris Flow	1.48	na	sandstone	6	0.077	0.031	37.894075°, -122.600199°
Twin Peaks Slide 1	Slump	1.61	12	chert	7	0.203	0.077	37.752615°, -122.448179°
Terra Linda Slide 1	Slump	1.63	25	serpentinite	8	0.130	0.046	38.020735°, -122.565233°
Terra Linda Slide 2	Slump/Debris Flow	1.44	79	sandstone/ serpentanite	7	0.232	0.088	38.021206°, -122.574540°
Roy's Redwood Preserve Slide 1	Slump	1.57	31	sandstone	8	0.138	0.049	38.015974°, -122.655866°

9.0 FIGURES

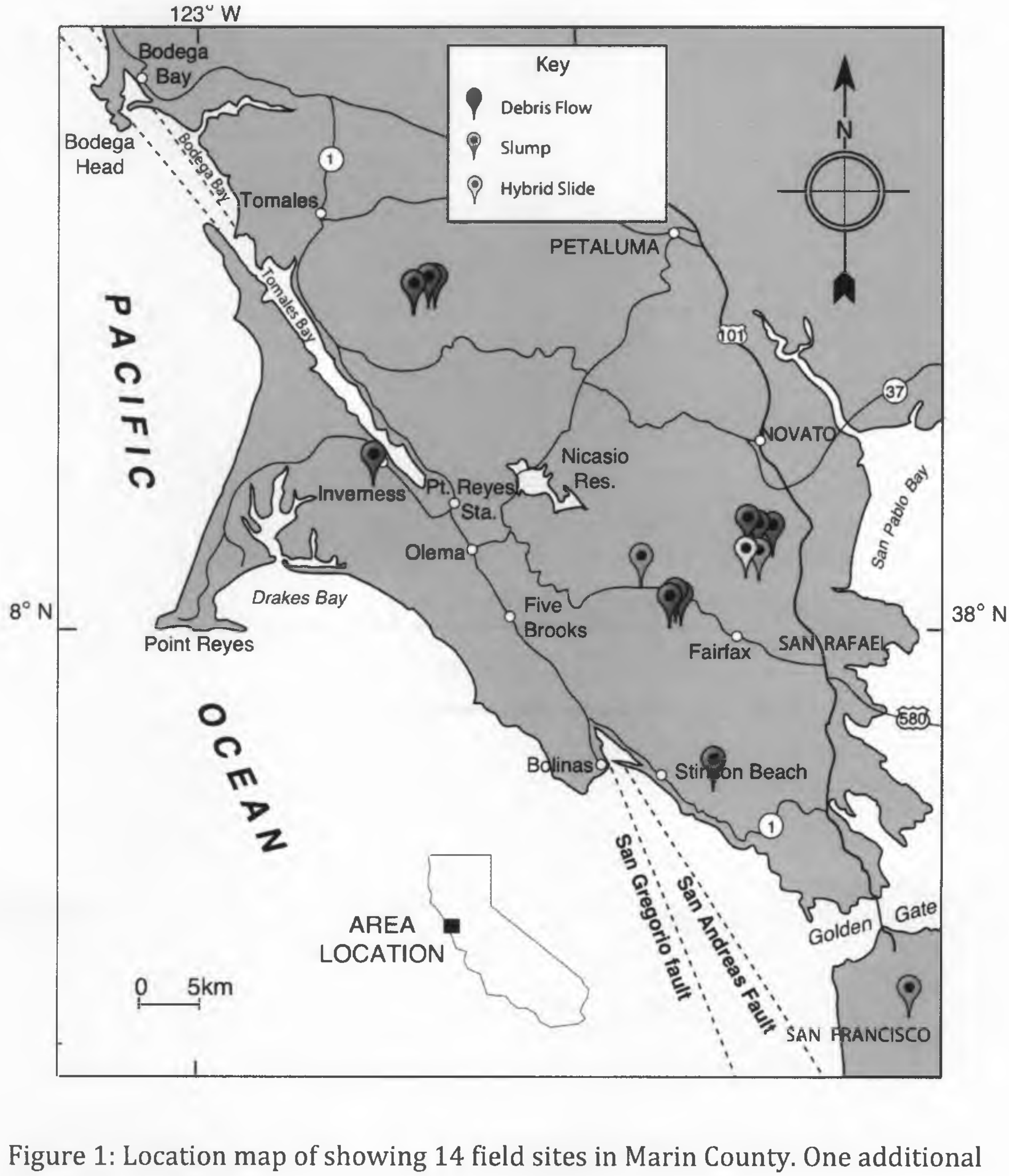

Figure 1: Location map of showing 14 field sites in Marin County. One additional landslide is in San Francisco. Adapted from Grove et al., 1995.

Figure 2: Photo of 2006 landslides that mobilized into debris flows in Briones Regional Park, Berkeley Hills, CA. Photo by Douglas Allen, used with permission of Dr. Jonathan Stock, USGS.

Figure 3: Typical slump flow off Highway 4 in Martinez, CA. Blocks of failed material remain within or just below headscarp. Cows for scale.

Figure 4: NASA's Mold Impression Laser Tool (MILT) with USGS template, a portable 3D scanner on custom platform in the field during bulk density measurement.

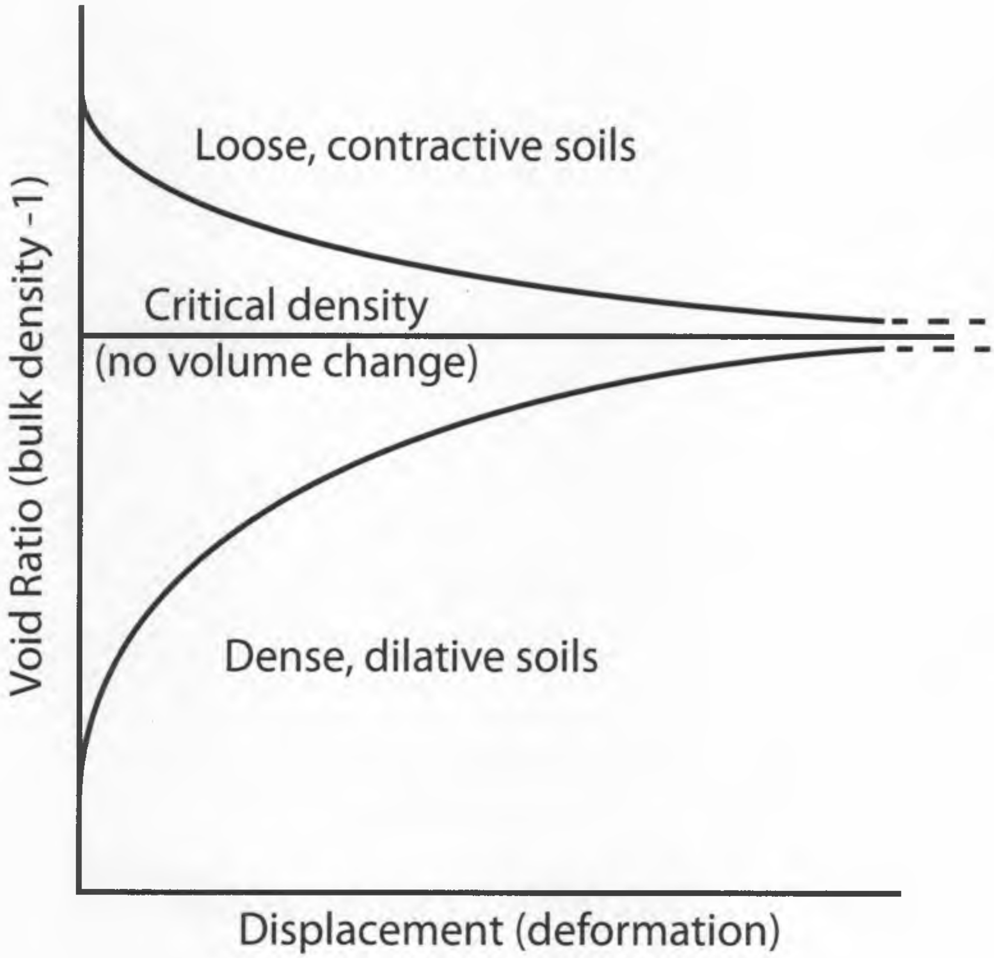

Figure 5: Change in void ratio (inverse of bulk density) of loose, low bulk density soils and dense, high bulk density soils during shear deformation from displacement during a direct shear test. Loose soils contract and dense soils dilate to reach a critical void ratio (or bulk density) during shear deformation. Adapted from Casagrande (1975).

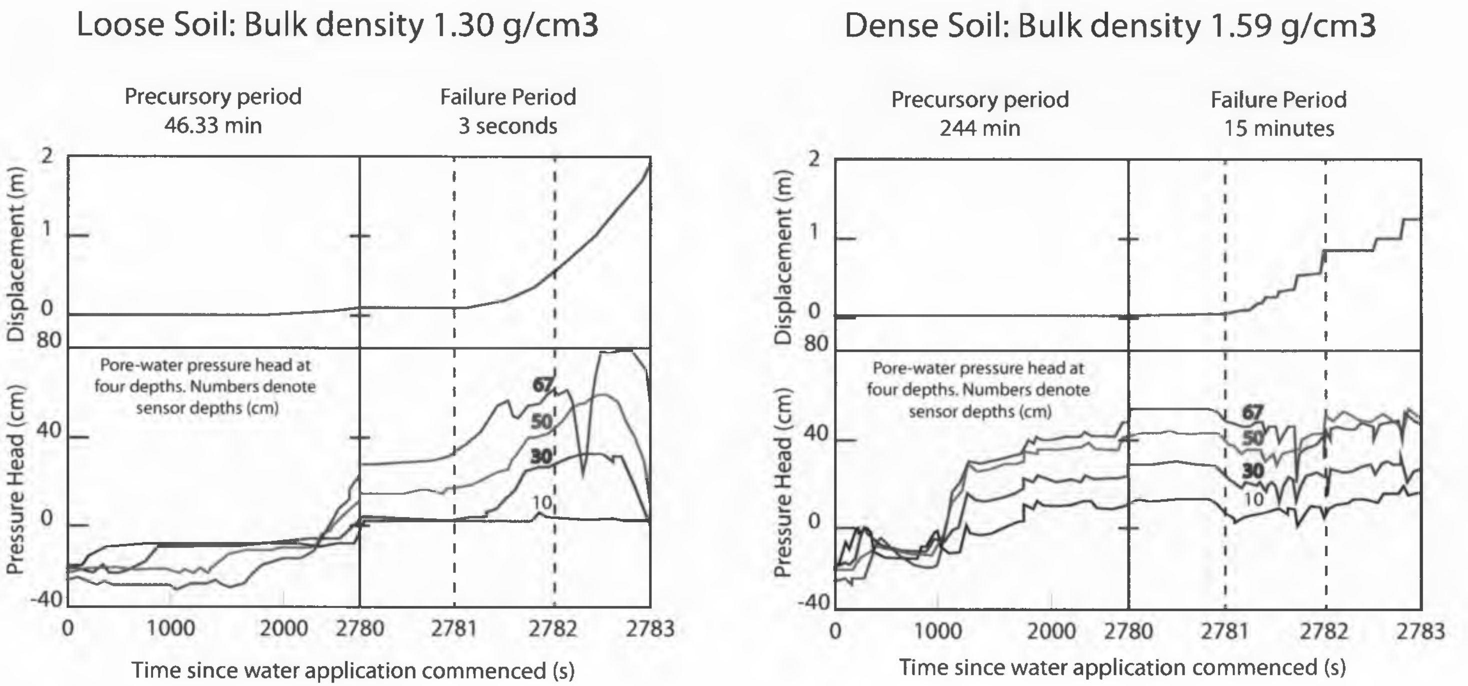

Figure 6: Displacement and pore pressure of loose (low bulk density) and dense (high bulk density) soils during artificial landslides showing contrasting dynamics. Loose soil sustained elevated pore pressure and material accelerated rapidly down-slope as a debris flow. Dense soil moved slowly and episodically with decreases in pore pressure during displacement and formed a slump. Adapted from Iverson et al., 2000.

Figure 7: MILT platform and soil sample in heat-resistant tin. Spikes on the bottom of the platform anchor it to the soil to maintain MILT's position between scans. Window in platform allows the MILT's lasers to image soil surface.

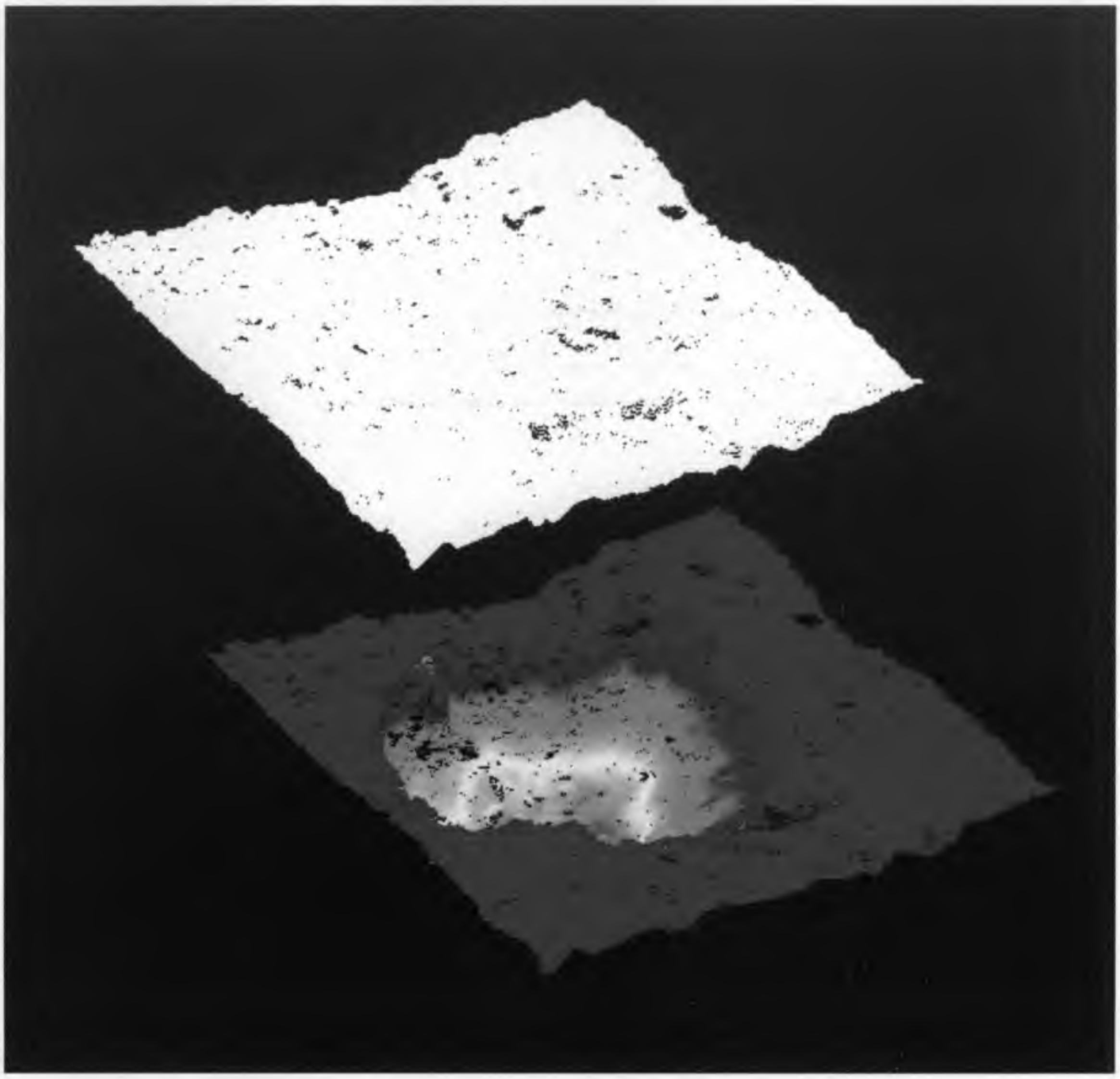

Figure 8: Screenshot of point-clouds from CloudCompare 2.6 showing initial scan (white) and final scan (color ramp) of the soil surface before and after taking soil sample. Scans are identical at edges allowing for the scans to be aligned and volume between them calculated. Black spots on point-clouds are areas of low point density.

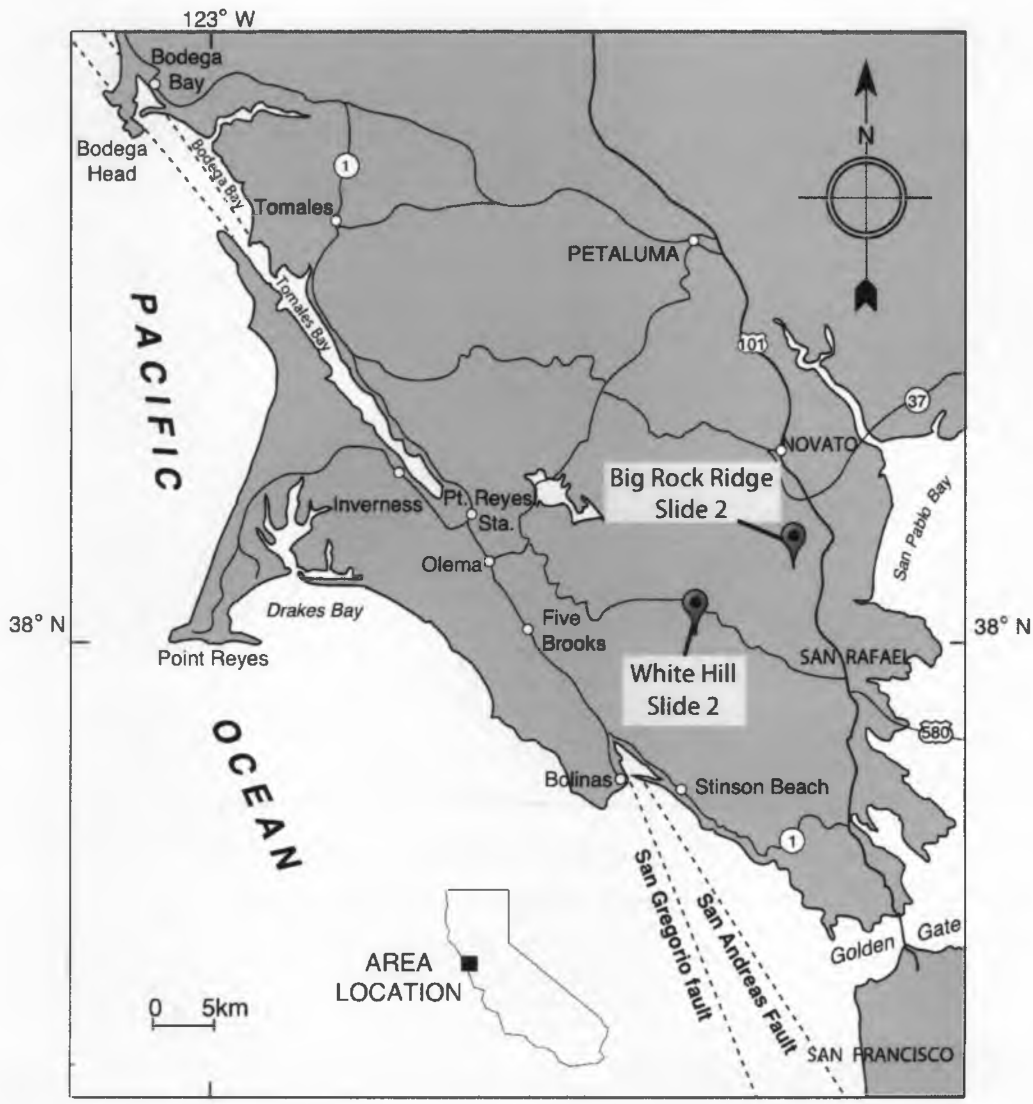

Figure 9: Location map of Big Rock Ridge Slide 2 and White Hill Slide 2. These landslides were sites of detailed sampling. Adapted from Grove et al., 1995.

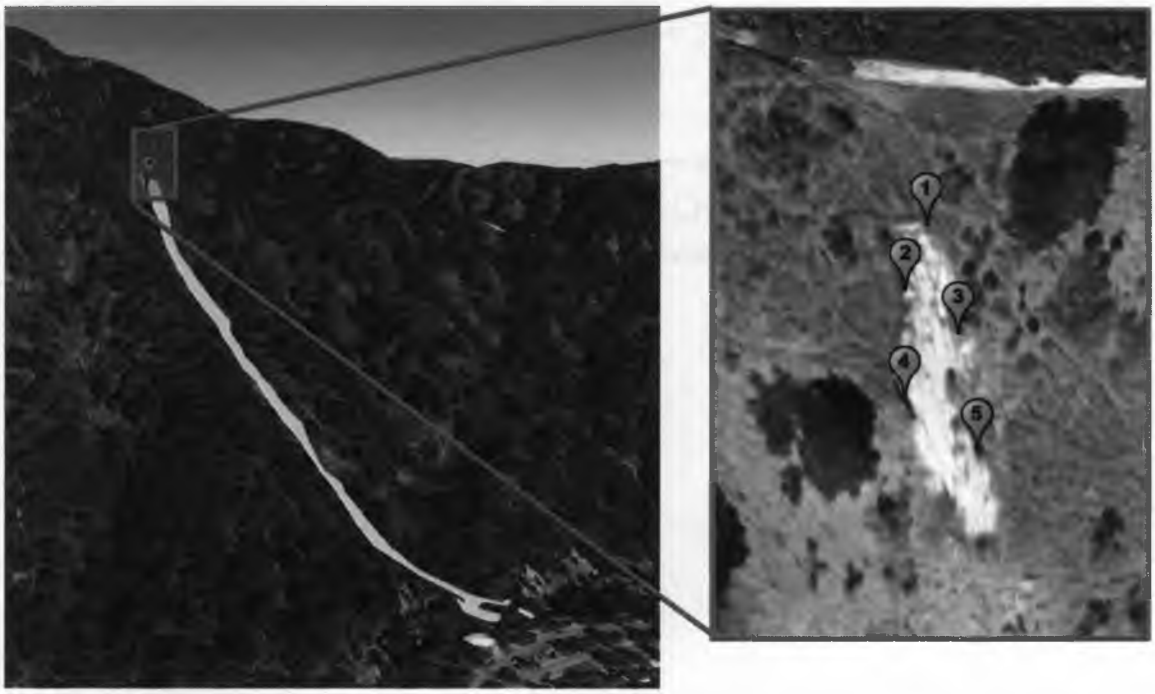

Figure 10: Aerial images of Big Rock Ridge Slide 2 showing debris flow runout from Stock and close-up of 5 sampling sites.

Figure 11: Photo of White Hill Slide 2 with location of sampling site on upper portion of lateral scarp.

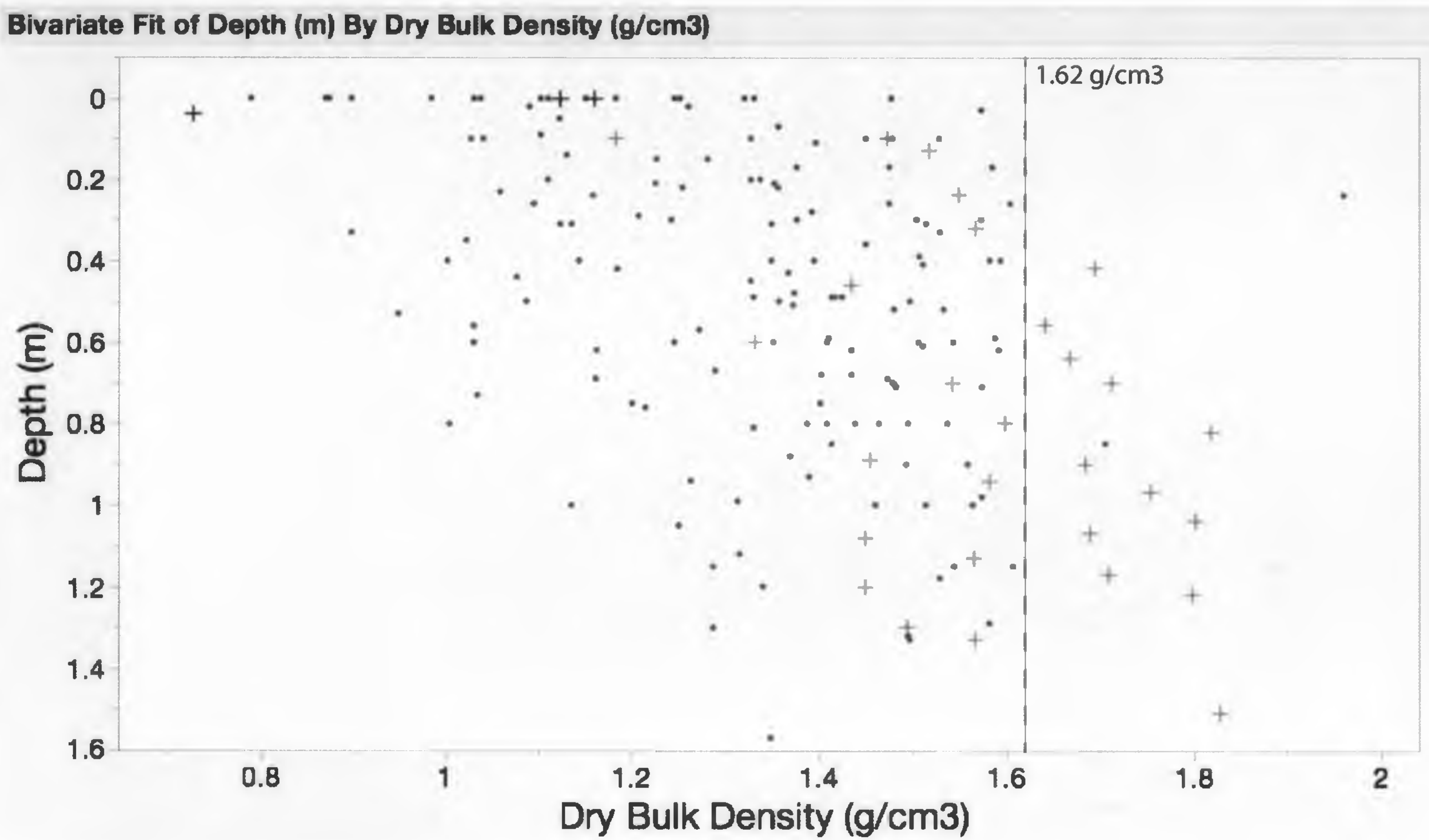

Figure 12: Plot of bulk density vs depth showing 178 bulk density measurements from 15 landslides. 31 measurements are from slumps (green crosses) and 147 are from debris flows (red dots). 26 surface measurements are in grey. 98% of debris flow measurements are below threshold of 1.62 g/cm^3, indicated by dashed red line.

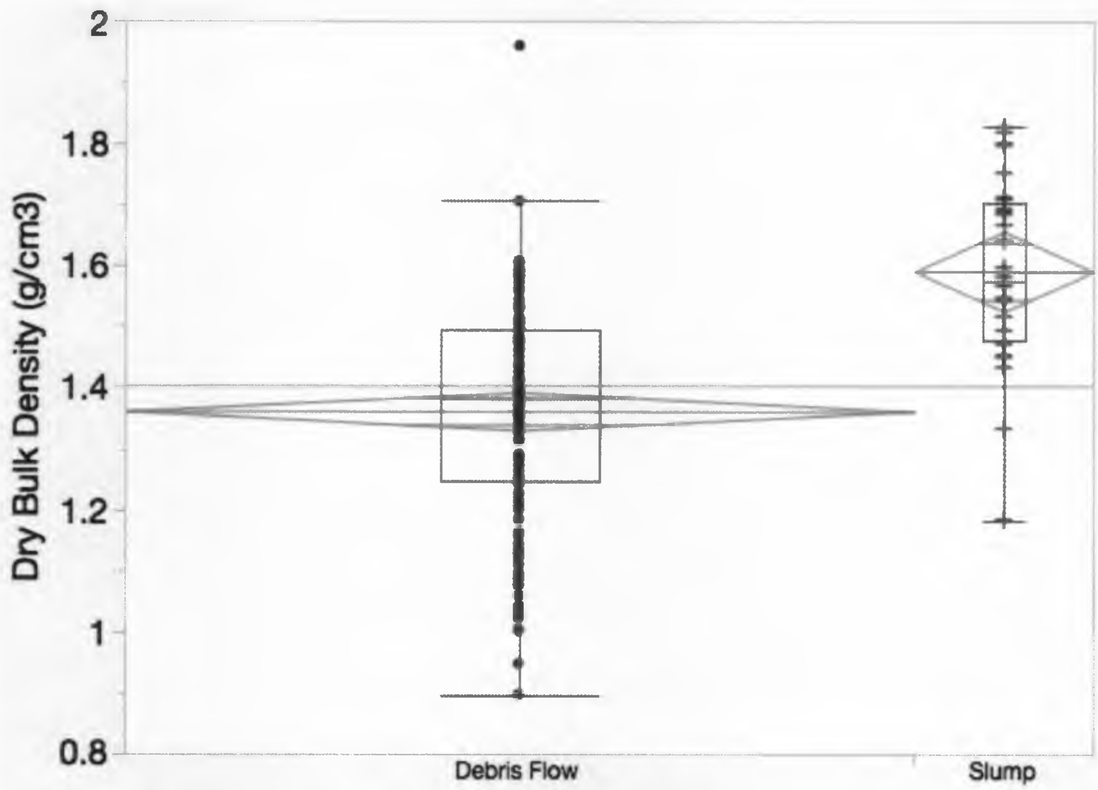

Figure 13: T-test comparing 124 bulk density measurements of soil at landslides that mobilized into debris flows (red dots) to 28 measurements of soil at slump sites (green crosses). Soils that slumped have a measurable different mean and median from soils that mobilized into debris flows. Debris flows = 1.36 +/- 0.016 g/cm^3; mean +/- S.E., slumps = 1.59 +/- 0.033 g/cm^3; mean +/- S.E., Prob > |t|=0.0001. Box and whisker plot shows median (center red line), upper and lower quantile (top and bottom of box, respectively) and upper and lower extremes, minus one outlier (whiskers). Center-line of green diamonds shows mean.

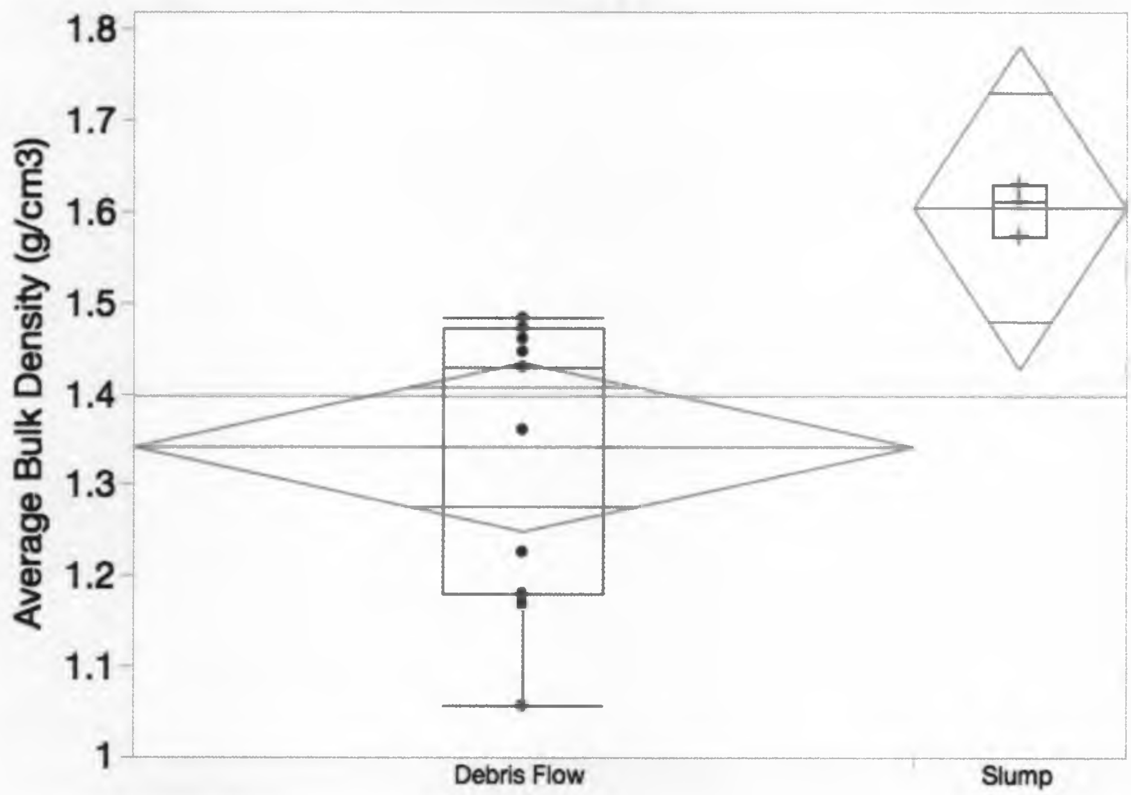

Figure 14: T-test comparing the average bulk density of 11 slide-averages from soils that mobilized into debris flows (red dots) to the average of 3 slide-averages of soils that slumped (green crosses). Soils that slumped have a measurably different mean and median from soils that mobilized into debris flows. Debris flows = 1.341 +/- 0.046 g/cm^3; mean +/- S.E.; mean +/- S.E., slumps = 1.604 +/- 0.016 g/cm^3; mean +/- S.E., Prob > |t|=0.0002. Box and whisker plot shows median (center red line), upper and lower quantile (top and bottom of box, respectively) and upper and lower extremes (whiskers). Center-line of green diamonds shows mean.

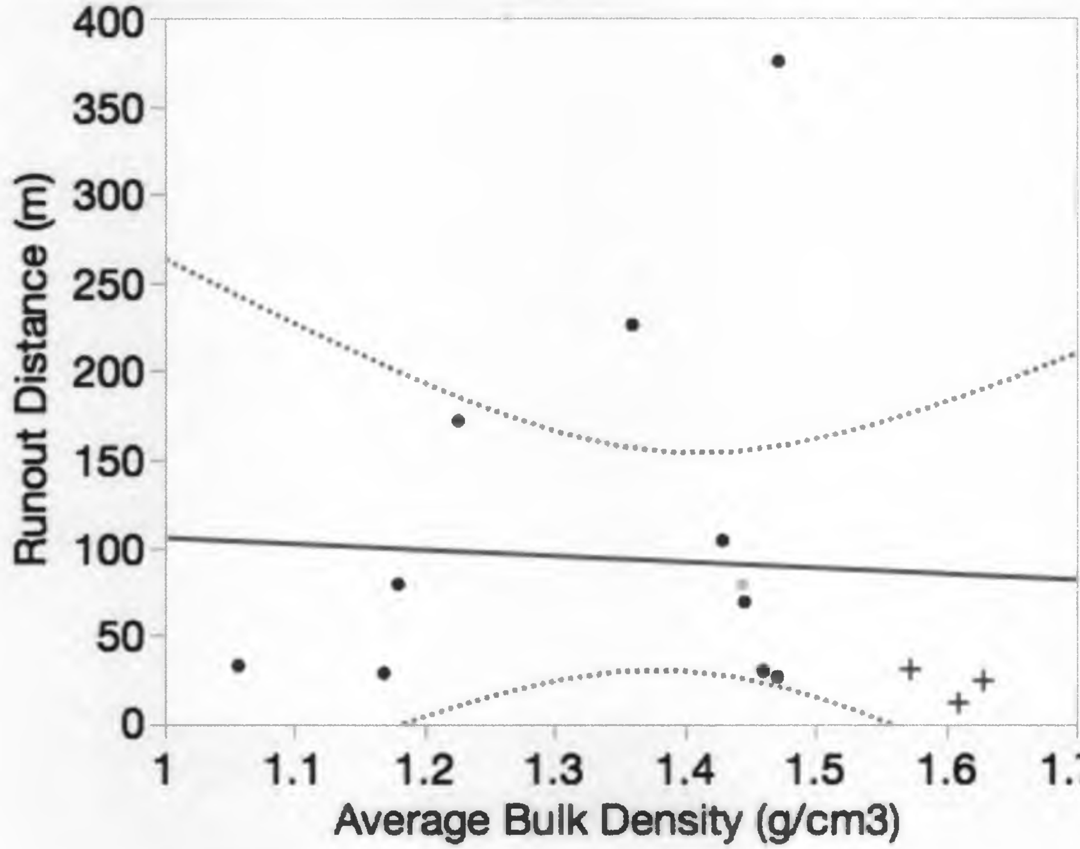

Figure 15: Linear regression of slide-average soil bulk density vs. runout length for 14 landslides shows no significant relationship between soil bulk density and runout distance.

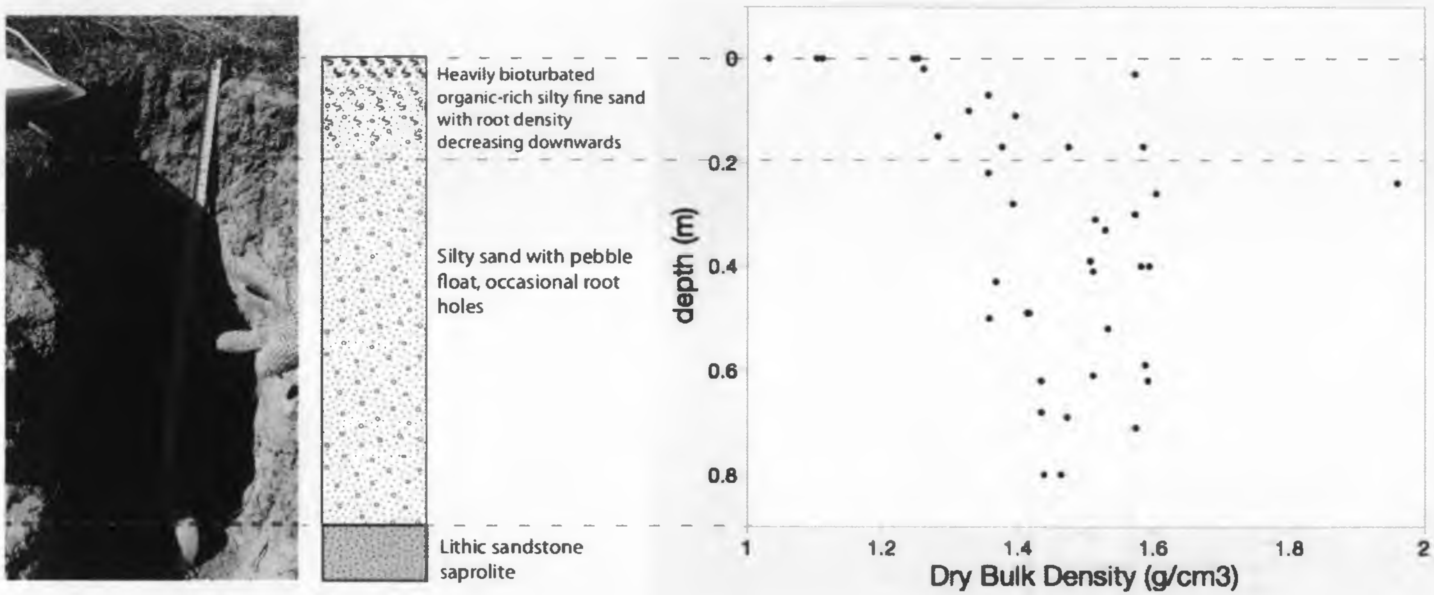

Figure 16: Photo of sample site 3, stratigraphic column and plot of bulk density vs. depth from Big Rock Ridge Slide 2 with depth from surface aligned in all 3 components. This slide has no stratification/soil horizons and no increase of bulk density with depth.

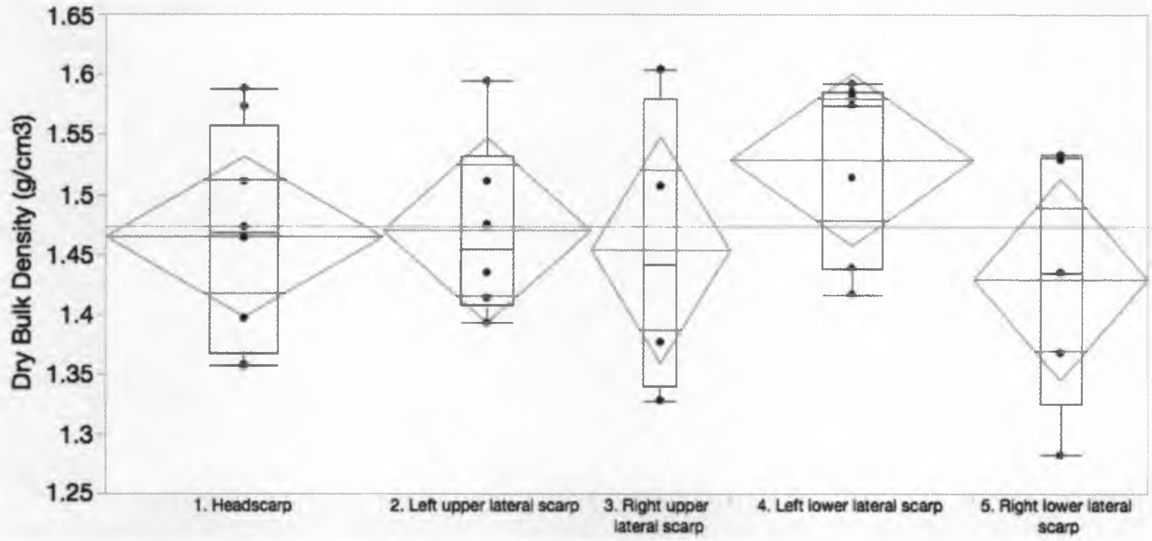

Figure 17: Bulk density measurements from 5 sites at Big Rock Ridge Slide 2. Upslope sites (towards the left in the plot) have less variability than downslope sites (toward the right in the plot) and average bulk densities close to the average bulk density for the entire scar (grey line). Surface measurements and one outlier excluded from this analysis. Box and whisker plot shows median (center red line), upper and lower quantile (top and bottom of box, respectively) and upper and lower extremes (whiskers). Center-line of green diamonds shows mean. Grey line shows mean bulk density for the entire landslide.

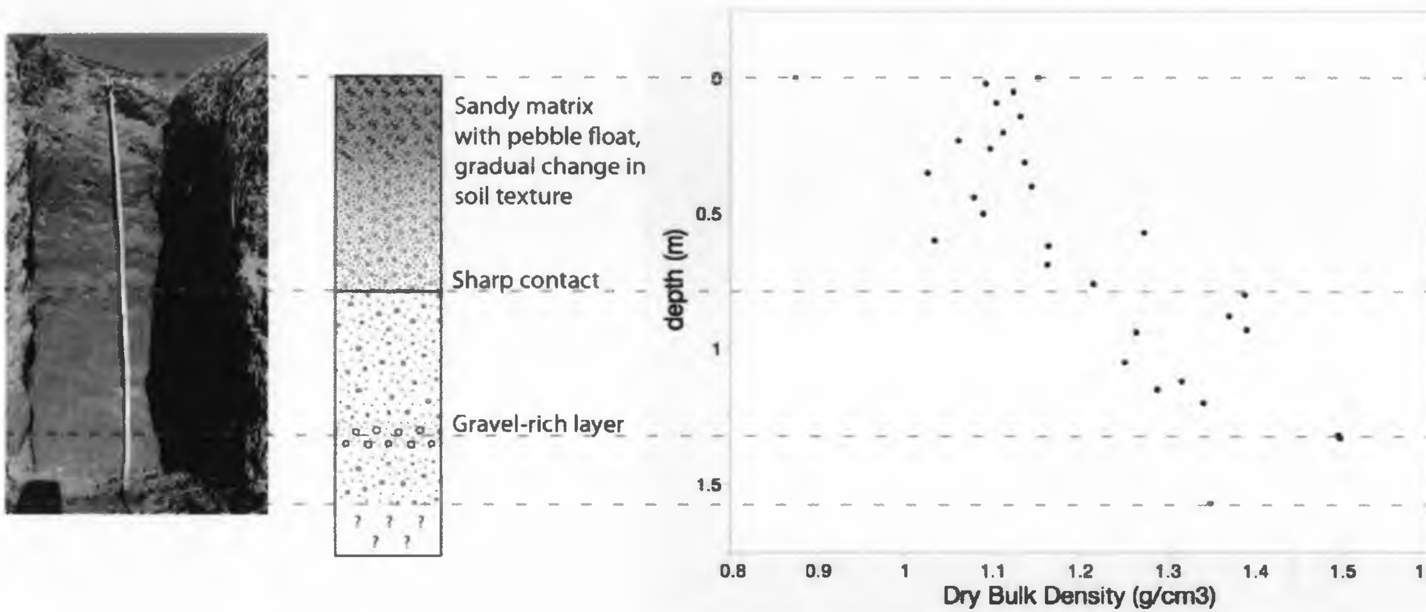

Figure 18: Photo of sample site, stratigraphic column and plot of bulk density vs depth from White Slide 2 with depth from surface aligned in all 3 components. This slide has stratified soil horizons and shows increased bulk density with depth. Greatest changes in bulk density occur across layer boundaries.

10.0 APPENDIX

Appendix 1 – CloudCompare Process

I used CloudCompare 2.6.0 to process the MILT scans and obtain the volume of the soil samples. For each sample I followed the following procedure (CloudCompare functions are in italics):

The MILT scans produce two text files associated with each soil sample: an initial scan before excavation and a final scan with the soil removed. I loaded both text files into CloudCompare, which converts them to point clouds. I perform the entire process with the view aligned with the Z axis, displaying the point clouds in map view. I select both clouds and choose *compute cloud/cloud distance*. I choose the initial cloud for the *reference* cloud and the final cloud as the *compared* cloud. I use the default settings for this function. This applies a color ramp to the final scan representing its distance from the original scan. The boundaries of the hole excavated in the soil become apparent.

With the hole illuminated by the color ramp, I use the *rectangular segment* tool to separate the portion of the scan containing the hole from the portion of the scans containing only the undisturbed, surrounding soil surface. The result is two pairs of clouds. The two "border" clouds, representing the undisturbed soil surface surrounding the hole are virtually identical. I use them to align the initial and final scans to correct for minor differences in the MILT's position between scans. I apply the *finely register roughly aligned entities* function to the two "border" clouds and select the "initial border" cloud as the *reference* and the "final border" cloud as the *data*. Again, I use CloudCompare's default settings. This function recognizes the similarities in these nearly identical clouds and shifts the "final border" cloud in space until the clouds are precisely aligned. In addition, CloudCompare produces a numerical log of the transformation that just took place. I copy this log and use the *apply transformation* function to shift the "final center" cloud (containing the hole), precisely aligning it with the "initial center" cloud (containing the soil surface before excavation). I then discard the pair of "border" clouds.

With the two "center" clouds aligned, I am able to calculate the volume contained between them. I use CloudCompare's *primitive factory* to create a virtual plane in space, parallel to the soil surface represented by the point clouds. I use the *compute cloud/mesh distance* function to calculate the average distance of each cloud from the plane. I then subtract the two distances and multiply the difference by the area of the cloud (Both clouds have identical areas in map view since they were both segmented in map view at the same time). The product is the volume of the space between the clouds, thus the volume of the soil sample excavated between scans.

Appendix 2 - Data Table

Location	Loc	Slide	site	sample	mass (g) field capacity sample & container	mass (g) after bake sample and container	Mass container(g)	Mass Sample Field Capacity (g)	Bulk Density Field (g/cm3; +/- 2%)	Mass Dry Sample (g)
Big Rock Ridge Slide 1	BRR	1	2	AB	51.17	48.50	21.49	29.68	1.27	27.01
	BRR	1	2	CD	48.36	45.76	21.52	26.84	1.61	24.24
	BRR	1	2	EF	64.86	61.30	21.28	43.58	1.37	40.02
	BRR	1	2	GH	49.53	49.00	21.15	28.38	1.53	27.85
	BRR	1	2	IJ	50.29	49.78	21.59	28.70	1.42	28.19
	BRR	1	2	KL	47.19	46.11	21.23	25.96	1.49	24.88
	BRR	1	2	MN	50.74	49.50	21.58	29.16	1.57	27.92
	BRR	1	2	OP	40.06	39.12	21.53	18.53	1.56	17.59
	BRR	1	2	QR	50.37	48.72	21.33	29.04	1.59	27.39
	BRR	1	2	ST	44.37	43.22	21.43	22.94	1.57	21.79
	BRR	1	2	WX	44.32	42.93	21.42	22.90	1.61	21.51
	BRR	1	2	YZ	54.74	52.68	21.58	33.16	1.65	31.10
Big Rock Ridge slide 2	BRR	2	1	AB	57.36	57.31	38.80	18.56	1.36	18.51
	BRR	2	1	CD	62.42	62.30	39.02	23.40	1.48	23.28
	BRR	2	1	EF	74.06	73.65	38.76	35.30	1.41	34.89
	BRR	2	1	GH	63.96	63.78	38.84	25.12	1.61	24.94
	BRR	2	1	IJ	69.25	68.81	38.77	30.48	1.43	30.04
	BRR	2	1	KL	61.73	61.44	38.75	22.98	1.53	22.69
	BRR	2	1	MN	75.29	74.51	38.97	36.32	1.47	35.54
	BRR	2	1	OP	39.22	39.00	21.27	17.95	1.13	17.73
	BRR	2	2	GH	43.60	43.39	21.48	22.12	1.11	21.91
	BRR	2	2	IJ	43.49	43.23	21.51	21.98	1.34	21.72
	BRR	2	2	AB	58.54	58.50	38.77	19.77	1.38	19.73
	BRR	2	2	CD	54.05	54.01	38.75	15.30	1.61	15.26
	BRR	2	2	EF	49.41	49.30	21.49	27.92	1.51	27.81
	BRR	2	3	QR	42.42	42.21	21.42	21.00	1.27	20.79
	BRR	2	3	AB	67.81	67.79	38.64	29.17	1.40	29.15
	BRR	2	3	CD	57.79	57.73	38.53	19.26	1.36	19.20

Location	Volume from CloudCompare (cm3)	Dry Bulk Density (g/cm3; +/- 2%)	Average Dry Bulk Density (g/cm3)	Average dry bulk density without surface meas. (g/cm3	depth (m)	Runout Distance (m)	% water	Debris Flow or slump
Big Rock Ridge Slide 1	23.460	1.15	1.434	1.460	0.00	30	9.00%	Debris Flow
	16.719	1.45	1.434	1.460	0.10	30	9.69%	Debris Flow
	31.900	1.25	1.434	1.460	0.22	30	8.17%	Debris Flow
	18.523	1.50	1.434	1.460	0.30	30	1.87%	Debris Flow
	20.201	1.40	1.434	1.460	0.40	30	1.78%	Debris Flow
	17.459	1.43	1.434	1.460	0.49	30	4.16%	Debris Flow
	18.538	1.51	1.434	1.460	0.60	30	4.25%	Debris Flow
	11.892	1.48	1.434	1.460	0.70	30	5.07%	Debris Flow
	18.319	1.50	1.434	1.460	0.80	30	5.68%	Debris Flow
	14.598	1.49	1.434	1.460	0.90	30	5.01%	Debris Flow
	14.212	1.51	1.434	1.460	1.00	30	6.07%	Debris Flow
	20.140	1.54	1.434	1.460	1.15	30	6.21%	Debris Flow
Big Rock Ridge slide 2	13.645	1.36	1.416	1.472	0.07	375	0.27%	Debris Flow
	15.787	1.47	1.416	1.472	0.17	375	0.51%	Debris Flow
	25.048	1.39	1.416	1.472	0.28	375	1.16%	Debris Flow
	15.647	1.59	1.416	1.472	0.40	375	0.72%	Debris Flow
	21.250	1.41	1.416	1.472	0.49	375	1.44%	Debris Flow
	15.016	1.51	1.416	1.472	0.61	375	1.26%	Debris Flow
	24.762	1.44	1.416	1.472	0.68	375	2.15%	Debris Flow
	15.955	1.11	1.416	1.472	0.00	375	1.23%	Debris Flow
	19.863	1.10	1.416	1.472	0.00	375	0.95%	Debris Flow
	16.354	1.33	1.416	1.472	0.10	375	1.18%	Debris Flow
	14.324	1.38	1.416	1.472	0.17	375	0.20%	Debris Flow
	9.514	1.60	1.416	1.472	0.26	375	0.26%	Debris Flow
	18.451	1.51	1.416	1.472	0.39	375	0.39%	Debris Flow
	16.600	1.25	1.416	1.472	0.00	375	1.00%	Debris Flow
	20.872	1.40	1.416	1.472	0.11	375	0.07%	Debris Flow
	14.152	1.36	1.416	1.472	0.22	375	0.31%	Debris Flow

Location	Loc	Slide	site	sample	mass (g) field capacity sample & container	mass (g) after bake sample and container	Mass container(g)	Mass Sample Field Capacity (g)	Bulk Density Field (g/cm3; +/- 2%)	Mass Dry Sample (g)
Big Rock Ridge Slide 2 Cont.	BRR	2	3	EF	58.37	58.24	38.67	19.70	1.58	19.57
	BRR	2	3	GH	59.25	59.04	38.95	20.30	1.53	20.09
	BRR	2	3	IJ	65.94	65.44	38.50	27.44	1.38	26.94
	BRR	2	3	KL	59.12	58.84	38.45	20.67	1.61	20.39
	BRR	2	3	MN	38.19	38.06	21.46	16.73	1.48	16.60
	BRR	2	3	OP	44.84	44.37	21.31	23.53	1.49	23.06
	BRR	2	4	QR	40.78	39.31	21.31	19.47	1.35	18.00
	BRR	2	4	AB	42.33	42.27	21.59	20.74	1.59	20.68
	BRR	2	4	CD	41.03	40.94	21.29	19.74	1.52	19.65
	BRR	2	4	EF	37.07	37.06	21.31	15.76	1.57	15.75
	BRR	2	4	GH	40.07	40.00	21.55	18.52	1.59	18.45
	BRR	2	4	IJ	50.94	50.66	21.35	29.59	1.43	29.31
	BRR	2	4	KL	44.90	44.66	21.36	23.54	1.61	23.30
	BRR	2	4	MN	40.89	40.72	21.43	19.46	1.59	19.29
	BRR	2	4	OP	43.11	42.81	21.43	21.68	1.46	21.38
	BRR	2	5	AB	36.41	36.39	21.25	15.16	1.26	15.14
	BRR	2	5	CD	40.97	40.94	21.35	19.62	1.28	19.59
	BRR	2	5	EF	38.39	38.37	21.59	16.80	1.96	16.78
	BRR	2	5	GH	54.06	53.90	21.15	32.91	1.54	32.75
	BRR	2	5	IJ	60.19	59.78	21.58	38.61	1.38	38.20
	BRR	2	5	KL	58.48	57.93	21.54	36.94	1.56	36.39
	BRR	2	5	MN	55.04	54.34	21.47	33.57	1.47	32.87
	BRR	2	5	OP	39.98	38.67	21.36	18.62	1.11	17.31
	BRR	2	1.1	AB	71.70	65.50	38.78	32.92	0.97	26.72
	BRR	2	1.1	CD	72.20	67.43	38.75	33.45	1.55	28.68
	BRR	2	1.1	EF	76.83	71.49	38.65	38.18	1.69	32.84
	BRR	2	1.1	GH	73.01	67.91	38.83	34.18	1.56	29.08
	BRR	2	1.1	IJ	74.33	69.36	38.89	35.44	1.50	30.47
	BRR	2	1.1	KL	76.53	70.57	38.52	38.01	1.68	32.05

Location	Volume from CloudCompare (cm3)	Dry Bulk Density (g/cm3; +/- 2%)	Average Dry Bulk Density (g/cm3)	Average dry bulk density without surface meas. (g/cm3	depth (m)	Runout Distance (m)	% water	Debris Flow or slump
Big Rock Ridge Slide 2 Cont.	12.438	1.57	1.416	1.472	0.30	375	0.66%	Debris Flow
	13.300	1.51	1.416	1.472	0.41	375	1.03%	Debris Flow
	19.840	1.36	1.416	1.472	0.50	375	1.82%	Debris Flow
	12.838	1.59	1.416	1.472	0.59	375	1.35%	Debris Flow
	11.270	1.47	1.416	1.472	0.69	375	0.78%	Debris Flow
	15.750	1.46	1.416	1.472	0.80	375	2.00%	Debris Flow
	14.452	1.25	1.416	1.472	0.00	375	7.55%	Debris Flow
	13.046	1.59	1.416	1.472	0.17	375	0.29%	Debris Flow
	12.980	1.51	1.416	1.472	0.31	375	0.46%	Debris Flow
	10.013	1.57	1.416	1.472	0.03	375	0.06%	Debris Flow
	11.665	1.58	1.416	1.472	0.40	375	0.38%	Debris Flow
	20.685	1.42	1.416	1.472	0.49	375	0.95%	Debris Flow
	14.640	1.59	1.416	1.472	0.62	375	1.02%	Debris Flow
	12.258	1.57	1.416	1.472	0.71	375	0.87%	Debris Flow
	14.853	1.44	1.416	1.472	0.80	375	1.38%	Debris Flow
	12.005	1.26	1.416	1.472	0.02	375	0.13%	Debris Flow
	15.280	1.28	1.416	1.472	0.15	375	0.15%	Debris Flow
	8.563	1.96	1.416	1.472	0.24	375	0.12%	Debris Flow
	21.414	1.53	1.416	1.472	0.33	375	0.49%	Debris Flow
	27.930	1.37	1.416	1.472	0.43	375	1.06%	Debris Flow
	23.732	1.53	1.416	1.472	0.52	375	1.49%	Debris Flow
	22.905	1.44	1.416	1.472	0.62	375	2.09%	Debris Flow
	16.781	1.03	1.416	1.472	0.00	375	7.04%	Debris Flow
	33.887	0.79	1.416	1.472	0.00	375	18.83%	Debris Flow
	21.589	1.33	1.416	1.472	0.20	375	14.26%	Debris Flow
	22.651	1.45	1.416	1.472	0.36	375	13.99%	Debris Flow
	21.851	1.33	1.416	1.472	0.49	375	14.92%	Debris Flow
	23.621	1.29	1.416	1.472	0.67	375	14.02%	Debris Flow
	22.664	1.41	1.416	1.472	0.85	375	15.68%	Debris Flow

Location	Loc	Slide	site	sample	mass (g) field capacity sample & container	mass (g) after bake sample and container	Mass container(g)	Mass Sample Field Capacity (g)	Bulk Density Field (g/cm3; +/- 2%)	Mass Dry Sample (g)
Big Rock Ridge Slide 3	BRR	3	2	AB	38.34	37.41	21.51	16.83	1.41	15.90
	BRR	3	2	CD	49.95	47.98	21.46	28.49	1.45	26.52
	BRR	3	2	EF	45.48	43.97	21.35	24.13	1.44	22.62
	BRR	3	2	GH	42.21	41.01	21.48	20.73	1.64	19.53
	BRR	3	2	IJ	48.35	46.70	21.42	26.93	1.50	25.28
	BRR	3	2	KL	42.09	40.86	21.27	20.82	1.67	19.59
White Hill Slide 1	WH	1	1	AB	62.08	58.25	38.99	23.09	1.25	19.26
	WH	1	1	CD	65.02	61.30	39.26	25.76	1.20	22.04
	WH	1	1	EF	55.14	49.06	21.40	33.74	1.50	27.66
	WH	1	1	GH	64.23	56.61	21.43	42.80	1.09	35.18
	WH	1	1	IJ	66.68	58.55	21.31	45.37	1.44	37.24
	WH	1	1	KL	52.58	45.87	20.99	31.59	1.20	24.88
White Hill Slide 2	WH	2	1	AB	53.80	48.11	21.38	32.42	1.06	26.73
	WH	2	1	CD	52.63	47.66	21.45	31.18	1.26	26.21
	WH	2	1	EF	52.41	46.69	21.48	30.93	1.40	25.21
	WH	2	1	IJ	52.16	46.73	21.43	30.73	1.41	25.30
	WH	2	1	KL	49.03	45.25	21.42	27.61	1.61	23.83
	WH	2	1	MN	56.60	51.99	21.30	35.30	1.60	30.69
	WH	2	1	OP	47.94	44.48	21.53	26.41	1.51	22.95
	WH	2	1	QR	57.59	52.64	21.14	36.45	1.73	31.50
	WH	2	1	ST	48.92	44.87	21.57	27.35	1.58	23.30
	WH	2	2.1	AB	49.56	46.15	22.37	27.19	1.32	23.78
	WH	2	2.1	CD	52.16	48.05	22.64	29.52	1.27	25.41
	WH	2	2.1	EF	50.29	46.20	22.47	27.82	1.32	23.73
	WH	2	2.1	GH	50.58	46.45	22.47	28.11	1.29	23.98
	WH	2	2.1	IJ	48.90	44.83	22.46	26.44	1.34	22.37
	WH	2	2.1	KL	49.14	44.41	22.40	26.74	1.35	22.01
	WH	2	2.1	MN	42.37	38.86	22.48	19.89	1.33	16.38
	WH	2	2.1	OP	52.60	47.75	22.10	30.50	1.35	25.65

Location	Volume from CloudCompare (cm3)	Dry Bulk Density (g/cm3; +/- 2%)	Average Dry Bulk Density (g/cm3)	Average dry bulk density without surface meas. (g/cm3	depth (m)	Runout Distance (m)	% water	Debris Flow or slump
Big Rock Ridge Slide 3	11.945	1.33	1.427	1.446	0.00	69	5.53%	Debris Flow
	19.605	1.35	1.427	1.446	0.21	69	6.91%	Debris Flow
	16.757	1.35	1.427	1.446	0.40	69	6.26%	Debris Flow
	12.660	1.54	1.427	1.446	0.60	69	5.79%	Debris Flow
	17.941	1.41	1.427	1.446	0.80	69	6.13%	Debris Flow
	12.446	1.57	1.427	1.446	0.98	69	5.91%	Debris Flow
White Hill Slide 1	18.530	1.04	1.054	1.057	0.00	33	16.59%	Debris Flow
	21.415	1.03	1.054	1.057	0.10	33	14.44%	Debris Flow
	22.553	1.23	1.054	1.057	0.21	33	18.02%	Debris Flow
	39.179	0.90	1.054	1.057	0.33	33	17.80%	Debris Flow
	31.424	1.19	1.054	1.057	0.42	33	17.92%	Debris Flow
	26.230	0.95	1.054	1.057	0.53	33	21.24%	Debris Flow
White Hill Slide 2	30.570	0.87	1.200	1.226	0.00	172	17.55%	Debris Flow
	24.724	1.06	1.200	1.226	0.23	172	15.94%	Debris Flow
	22.039	1.14	1.200	1.226	0.40	172	18.49%	Debris Flow
	21.747	1.16	1.200	1.226	0.62	172	17.67%	Debris Flow
	17.170	1.39	1.200	1.226	0.80	172	13.69%	Debris Flow
	22.078	1.39	1.200	1.226	0.93	172	13.06%	Debris Flow
	17.433	1.32	1.200	1.226	1.12	172	13.10%	Debris Flow
	21.070	1.50	1.200	1.226	1.32	172	13.58%	Debris Flow
	17.271	1.35	1.200	1.226	1.57	172	14.81%	Debris Flow
	20.668	1.15	1.200	1.226	0.00	172	12.54%	Debris Flow
	23.297	1.09	1.200	1.226	0.02	172	13.92%	Debris Flow
	21.126	1.12	1.200	1.226	0.05	172	14.70%	Debris Flow
	21.742	1.10	1.200	1.226	0.09	172	14.69%	Debris Flow
	19.780	1.13	1.200	1.226	0.14	172	15.39%	Debris Flow
	19.818	1.11	1.200	1.226	0.20	172	17.69%	Debris Flow
	14.943	1.10	1.200	1.226	0.26	172	17.65%	Debris Flow
	22.582	1.14	1.200	1.226	0.31	172	15.90%	Debris Flow

Location	Loc	Slide	site	sample	mass (g) field capacity sample & container	mass (g) after bake sample and container	Mass container(g)	Mass Sample Field Capacity (g)	Bulk Density Field (g/cm3; +/- 2%)	Mass Dry Sample (g)
White Hill Slide 2 Cont.	WH	2	2.1	QR	52.29	47.04	22.52	29.77	1.24	24.52
	WH	2	2.1	ST	47.59	43.25	22.29	25.30	1.30	20.96
	WH	2	2.1	UV	48.19	43.24	22.12	26.07	1.34	21.12
	WH	2	2.1	WX	40.60	37.63	22.11	18.49	1.52	15.52
	WH	2	2.1	YZ	39.69	36.95	21.88	17.81	1.22	15.07
	WH	2	2.1	ZA,ZB	42.99	39.46	21.98	21.01	1.40	17.48
	WH	2	2.1	ZC,ZD	45.92	42.22	21.87	24.05	1.44	20.35
	WH	2	2.1	ZE,ZF	49.23	45.23	22.34	26.89	1.61	22.89
	WH	2	2.1	ZG,ZH	45.05	41.00	22.57	22.48	1.54	18.43
	WH	2	2.1	ZI,ZJ	43.84	40.38	22.28	21.56	1.49	18.10
	WH	2	2.1	ZK,ZL	50.05	45.35	22.60	27.45	1.55	22.75
	WH	2	2.1	ZM,ZN	45.27	41.48	22.35	22.92	1.61	19.13
	WH	2	2.1	ZO,ZP	44.59	41.29	22.27	22.32	1.76	19.02
White Hill Slide 3	WH	3	1	AB	51.56	45.15	21.34	30.22	1.25	23.81
	WH	3	1	CD	52.19	46.04	21.55	30.64	1.45	24.49
	WH	3	1	EF	52.48	46.54	21.57	30.91	1.24	24.97
	WH	3	1	GH	53.06	47.00	21.42	31.64	1.54	25.58
	WH	3	1	IJ	57.58	50.36	21.29	36.29	1.66	29.07
	WH	3	1	KL	49.56	44.44	21.25	28.31	1.60	23.19
	WH	3	2	AB	45.92	41.20	21.47	24.45	1.11	19.73
	WH	3	2	DE	46.44	42.04	21.37	25.07	1.36	20.67
	WH	3	2	FG	71.28	64.73	38.67	32.61	1.26	26.06
Walker Ranch Slide 1	WR	1	2	CD	75.62	69.43	38.80	36.82	1.61	30.63
	WR	1	2	EF	82.43	75.80	38.77	43.66	1.59	37.03
	WR	1	2	GH	72.34	67.42	38.76	33.58	1.65	28.66
	WR	1	2	IJ	74.81	68.90	38.97	35.84	1.84	29.93
	WR	1	2	KL	74.70	68.12	39.06	35.64	1.79	29.06
	WR	1	2	MN	68.49	62.74	38.73	29.76	1.94	24.01
Walker Ranch Slide 2	WR	2	2	AB	62.01	57.58	38.83	23.18	1.08	18.75

Location	Volume from CloudCompare (cm3)	Dry Bulk Density (g/cm3; +/- 2%)	Average Dry Bulk Density (g/cm3)	Average dry bulk density without surface meas. (g/cm3	depth (m)	Runout Distance (m)	% water	Debris Flow or slump
White Hill Slide 2 Cont.	23.946	1.02	1.200	1.226	0.35	172	17.64%	Debris Flow
	19.444	1.08	1.200	1.226	0.44	172	17.15%	Debris Flow
	19.416	1.09	1.200	1.226	0.50	172	18.99%	Debris Flow
	12.192	1.27	1.200	1.226	0.57	172	16.06%	Debris Flow
	14.608	1.03	1.200	1.226	0.60	172	15.38%	Debris Flow
	15.047	1.16	1.200	1.226	0.69	172	16.80%	Debris Flow
	16.753	1.21	1.200	1.226	0.76	172	15.38%	Debris Flow
	16.704	1.37	1.200	1.226	0.88	172	14.88%	Debris Flow
	14.579	1.26	1.200	1.226	0.94	172	18.02%	Debris Flow
	14.474	1.25	1.200	1.226	1.05	172	16.05%	Debris Flow
	17.657	1.29	1.200	1.226	1.15	172	17.12%	Debris Flow
	14.267	1.34	1.200	1.226	1.20	172	16.54%	Debris Flow
	12.707	1.50	1.200	1.226	1.33	172	14.78%	Debris Flow
White Hill Slide 3	24.161	0.99	1.118	1.169	0.00	29	21.21%	Debris Flow
	21.132	1.16	1.118	1.169	0.24	29	20.07%	Debris Flow
	24.900	1.00	1.118	1.169	0.40	29	19.22%	Debris Flow
	20.527	1.25	1.118	1.169	0.60	29	19.15%	Debris Flow
	21.841	1.33	1.118	1.169	0.81	29	19.90%	Debris Flow
	17.653	1.31	1.118	1.169	0.99	29	18.09%	Debris Flow
	21.970	0.90	1.118	1.169	0.00	29	19.30%	Debris Flow
	18.392	1.12	1.118	1.169	0.31	29	17.55%	Debris Flow
	25.922	1.01	1.118	1.169	0.80	29	20.09%	Debris Flow
Walker Ranch Slide 1	22.896	1.34	1.443	1.443	0.20	104	16.81%	Debris Flow
	27.433	1.35	1.443	1.443	0.40	104	15.19%	Debris Flow
	20.345	1.41	1.443	1.443	0.60	104	14.65%	Debris Flow
	19.472	1.54	1.443	1.443	0.80	104	16.49%	Debris Flow
	19.903	1.46	1.443	1.443	1.00	104	18.46%	Debris Flow
	15.352	1.56	1.443	1.443	1.00	104	19.32%	Debris Flow
Walker Ranch Slide 2	21.549	0.87	1.405	1.471	0.00	27	19.11%	Debris Flow

Location	Loc	Slide	site	sample	mass (g) field capacity sample & container	mass (g) after bake sample and container	Mass container(g)	Mass Sample Field Capacity (g)	Bulk Density Field (g/cm3; +/- 2%)	Mass Dry Sample (g)
Walker Ranch Slide 2 Cont.	WR	2	2	CD	67.73	63.58	38.80	28.93	1.78	24.78
	WR	2	2	EF	60.99	57.83	38.38	22.61	1.60	19.45
	WR	2	2	GH	83.93	77.68	38.85	45.08	1.74	38.83
	WR	2	2	IJ	65.42	62.56	38.73	26.69	1.57	23.83
	WR	2	2	KL	57.79	55.91	38.94	18.85	1.90	16.97
	WR	2	2	MN	69.68	65.68	39.02	30.66	1.70	26.66
	WR	2	2	OP	70.73	66.44	38.82	31.91	1.59	27.62
	WR	2	2	QR	74.04	69.62	38.74	35.30	1.61	30.88
Walker Ranch Slide 3	WR	3.1	1	AB	75.64	69.20	38.81	36.83	1.43	30.39
	WR	3	1	CD	76.21	69.44	39.17	37.04	1.50	30.27
	WR	3	1	EF	79.65	73.08	39.00	40.65	1.48	34.08
	WR	3	1	GH	104.44	93.94	38.49	65.95	1.58	55.45
	WR	3	1	IJ	77.98	71.64	38.62	39.36	1.61	33.02
	WR	3	1	KL	73.14	67.47	39.06	34.08	1.44	28.41
	WR	3	1	MN	80.85	74.76	38.80	42.05	1.82	35.96
	WR	3	1	OP	80.38	74.31	38.45	41.93	1.88	35.86
Point Reyes Slide 1	PR	1	1	AB	38.92	36.93	22.35	16.57	1.18	14.58
	PR	1	1	CD	49.96	46.30	22.40	27.56	1.39	23.90
	PR	1	1	EF	56.46	52.47	22.31	34.15	1.55	30.16
	PR	1	1	GH	52.42	48.67	22.52	29.90	1.18	26.15
	PR	1	1	IJ	41.40	39.09	22.42	18.98	1.29	16.67
	PR	1	1	KL	52.64	49.26	22.41	30.23	1.45	26.85
Twin Peaks Slide 1	TP	1	1.0	CD	44.57	41.53	22.11	22.46	1.37	19.42
	TP	1	1.0	EF	47.64	44.17	21.98	25.66	1.79	22.19
	TP	1	1.0	GH	51.70	48.10	22.48	29.22	1.93	25.62
	TP	1	1.0	IJ	53.91	49.69	22.41	31.50	1.90	27.28
	TP	1	1.0	KL	48.81	45.10	21.98	26.83	1.99	23.12
	TP	1	1.0	MN	46.45	43.21	22.26	24.19	1.95	20.95
	TP	1	1.0	OP	46.93	43.62	22.38	24.55	2.08	21.24

Location	Volume from CloudCompare (cm3)	Dry Bulk Density (g/cm3; +/- 2%)	Average Dry Bulk Density (g/cm3)	Average dry bulk density without surface meas. (g/cm3	depth (m)	Runout Distance (m)	% water	Debris Flow or slump
Walker Ranch Slide 2 Cont.	16.222	1.53	1.405	1.471	0.10	27	14.34%	Debris Flow
	14.123	1.38	1.405	1.471	0.30	27	13.98%	Debris Flow
	25.946	1.50	1.405	1.471	0.50	27	13.86%	Debris Flow
	16.979	1.40	1.405	1.471	0.68	27	10.72%	Debris Flow
	9.945	1.71	1.405	1.471	0.85	27	9.97%	Debris Flow
	18.075	1.47	1.405	1.471	0.26	27	13.05%	Debris Flow
	20.107	1.37	1.405	1.471	0.48	27	13.44%	Debris Flow
	21.882	1.41	1.405	1.471	0.59	27	12.52%	Debris Flow
Walker Ranch Slide 3	25.697	1.18	1.337	1.360	0.00	226	17.49%	Debris Flow
	24.665	1.23	1.337	1.360	0.15	226	18.28%	Debris Flow
	27.417	1.24	1.337	1.360	0.30	226	16.16%	Debris Flow
	41.753	1.33	1.337	1.360	0.45	226	15.92%	Debris Flow
	24.432	1.35	1.337	1.360	0.60	226	16.11%	Debris Flow
	23.651	1.20	1.337	1.360	0.75	226	16.64%	Debris Flow
	23.071	1.56	1.337	1.360	0.90	226	14.48%	Debris Flow
	22.313	1.61	1.337	1.360	1.15	226	14.48%	Debris Flow
Point Reyes Slide 1	13.989	1.04	1.180	1.180	0.10	79	12.01%	Debris Flow
	19.791	1.21	1.180	1.180	0.29	79	13.28%	Debris Flow
	21.971	1.37	1.180	1.180	0.51	79	11.68%	Debris Flow
	25.252	1.04	1.180	1.180	0.73	79	12.54%	Debris Flow
	14.672	1.14	1.180	1.180	1.00	79	12.17%	Debris Flow
	20.841	1.29	1.180	1.180	1.30	79	11.18%	Debris Flow
Twin Peaks Slide 1	16.399	1.18	1.610	1.610	0.10	12	13.54%	Slump
	14.334	1.55	1.610	1.610	0.24	12	13.52%	Slump
	15.125	1.69	1.610	1.610	0.42	12	12.32%	Slump
	16.615	1.64	1.610	1.610	0.56	12	13.40%	Slump
	13.496	1.71	1.610	1.610	0.70	12	13.83%	Slump
	12.433	1.69	1.610	1.610	0.90	12	13.39%	Slump
	11.792	1.80	1.610	1.610	1.04	12	13.48%	Slump

Location	Loc	Slide	site	sample	mass (g) field capacity sample & container	mass (g) after bake sample and container	Mass container(g)	Mass Sample Field Capacity (g)	Bulk Density Field (g/cm3; +/- 2%)	Mass Dry Sample (g)
Terra Linda Slide 1	TL	1	1.0	AB	42.79	38.15	22.22	20.57	0.94	15.93
	TL	1	1.0	CD	49.64	45.66	21.74	27.90	1.77	23.92
	TL	1	1.0	EF	50.08	46.12	21.90	28.18	1.82	24.22
	TL	1	1.0	GH	49.67	45.46	22.00	27.67	1.69	23.46
	TL	1	1.0	IJ	49.33	45.06	22.08	27.25	1.98	22.98
	TL	1	1.0	KL	53.93	49.49	22.14	31.79	2.11	27.35
	TL	1	1.0	MN	57.87	52.52	22.00	35.87	2.06	30.52
	TL	1	1.0	OP	49.96	46.11	22.14	27.82	1.98	23.97
	TL	1	1.0	QR	50.60	46.30	22.21	28.39	1.85	24.09
Roys Redwood Presv. Slide 1	RR	1	1.0	AB	44.70	40.84	21.88	22.82	1.35	18.96
	RR	1	1.0	CD	42.05	39.21	21.32	20.73	1.71	17.89
	RR	1	1.0	EF	64.57	56.08	21.40	43.17	1.66	34.68
	RR	1	1.0	GH	61.47	53.43	22.01	39.46	1.94	31.42
	RR	1	1.0	IJ	60.78	54.17	21.00	39.78	1.92	33.17
	RR	1	1.0	KL	56.80	51.68	21.36	35.44	1.85	30.32
	RR	1	1.0	MN	51.17	47.41	21.44	29.73	1.93	25.97
	RR	1	1.0	OP	52.44	48.17	21.47	30.97	1.82	26.70
	RR	1	1.0	QR	52.41	48.28	21.42	30.99	2.07	26.86
Terra Linda Slide 2	Tl	2	1.0	AB	50.88	47.53	22.01	28.87	1.49	25.52
	Tl	2	1.0	CD	48.91	44.03	22.06	26.85	1.26	21.97
	Tl	2	1.0	EF	48.91	44.45	21.15	27.76	1.67	23.30
	Tl	2	1.0	GH	44.68	40.25	21.45	23.23	1.80	18.80
	Tl	2	1.0	IJ	40.03	36.70	21.51	18.52	1.77	15.19
	Tl	2	1.0	KL	45.11	41.05	21.45	23.66	1.75	19.60
	Tl	2	1.0	MN	52.83	47.80	21.43	31.40	1.78	26.37
	Tl	2	1.0	OP	57.42	53.01	21.59	35.83	2.08	31.42
Mount Tamalpais Slide 1	MT	1	1.0	AB	47.05	45.45	21.27	25.78	1.57	24.18
	MT	1	1.0	CD	45.26	43.21	21.47	23.79	1.62	21.74
	MT	1	1.0	EF	48.46	45.27	21.41	27.05	1.53	23.86

Location	Volume from CloudCompare (cm3)	Dry Bulk Density (g/cm3; +/- 2%)	Average Dry Bulk Density (g/cm3)	Average dry bulk density without surface meas. (g/cm3	depth (m)	Runout Distance (m)	% water	Debris Flow or slump
Terra Linda Slide 1	21.897	0.73	1.529	1.629	0.04	25	22.56%	Slump
	15.771	1.52	1.529	1.629	0.13	25	14.27%	Slump
	15.458	1.57	1.529	1.629	0.32	25	14.05%	Slump
	16.361	1.43	1.529	1.629	0.46	25	15.22%	Slump
	13.789	1.67	1.529	1.629	0.64	25	15.67%	Slump
	15.036	1.82	1.529	1.629	0.82	25	13.97%	Slump
	17.413	1.75	1.529	1.629	0.97	25	14.91%	Slump
	14.026	1.71	1.529	1.629	1.17	25	13.84%	Slump
	15.375	1.57	1.529	1.629	1.33	25	15.15%	Slump
Roys Redwood Presv.	16.869	1.12	1.523	1.573	0.00	31	16.91%	Slump
Slide 1	12.155	1.47	1.523	1.573	0.10	31	13.70%	Slump
	26.016	1.33	1.523	1.573	0.60	31	19.67%	Slump
	20.371	1.54	1.523	1.573	0.70	31	20.38%	Slump
	20.756	1.60	1.523	1.573	0.80	31	16.62%	Slump
	19.160	1.58	1.523	1.573	0.94	31	14.45%	Slump
	15.373	1.69	1.523	1.573	1.07	31	12.65%	Slump
	17.054	1.57	1.523	1.573	1.13	31	13.79%	Slump
	14.940	1.80	1.523	1.573	1.22	31	13.33%	Slump
Terra Linda Slide 2	19.321	1.32	1.429	1.444	0.00	79	11.60%	Hybrid Slide
	21.299	1.03	1.429	1.444	0.56	79	18.18%	Hybrid Slide
	16.616	1.40	1.429	1.444	0.75	79	16.07%	Hybrid Slide
	12.934	1.45	1.429	1.444	0.89	79	19.07%	Hybrid Slide
	10.474	1.45	1.429	1.444	1.08	79	17.98%	Hybrid Slide
	13.516	1.45	1.429	1.444	1.20	79	17.16%	Hybrid Slide
	17.650	1.49	1.429	1.444	1.30	79	16.02%	Hybrid Slide
	17.191	1.83	1.429	1.444	1.51	79	12.31%	Hybrid Slide
Mount Tamalpais	16.376	1.48	1.483	1.484	0.00	na	6.21%	Debris Flow
Slide 1	14.712	1.48	1.483	1.484	0.10	na	8.62%	Debris Flow
	17.669	1.35	1.483	1.484	0.31	na	11.79%	Debris Flow

Location	Loc	Slide	site	sample	mass (g) field capacity sample & container	mass (g) after bake sample and container	Mass container(g)	Mass Sample Field Capacity (g)	Bulk Density Field (g/cm3; +/- 2%)	Mass Dry Sample (g)
Mount Tamalpais	MT	1	1.0	GH	46.14	43.15	21.35	24.79	1.68	21.80
Slide 1 cont.	MT	1	1.0	IJ	44.39	41.44	21.30	23.09	1.70	20.14
	MT	1	1.0	KL	42.65	39.73	21.96	20.69	1.78	17.77
	MT	1	1.0	MN	42.19	39.26	21.56	20.63	1.84	17.70

Location	Volume from CloudCompare (cm3)	Dry Bulk Density (g/cm3; +/- 2%)	Average Dry Bulk Density (g/cm3)	Average dry bulk density without surface meas. (g/cm3	depth (m)	Runout Distance (m)	% water	Debris Flow or slump
Mount Tamalpais	14.732	1.48	1.483	1.484	0.52	na	12.06%	Debris Flow
Slide 1 cont.	13.586	1.48	1.483	1.484	0.71	na	12.78%	Debris Flow
	11.622	1.53	1.483	1.484	1.18	na	14.11%	Debris Flow
	11.185	1.58	1.483	1.484	1.29	na	14.20%	Debris Flow

Appendix 3 - Excluded Data

Location	Loc	Slide	site	sample	mass (g) field capacity sample & container	mass (g) after bake sample and container	Mass container(g)	Mass Sample Field Capacity (g)	Bulk Density Field (g/cm3; +/- 2%)	Mass Dry Sample (g)
Walker Ranch Slide 1	WR	1	1.0	A	61.07	60.79	39.01			
	WR	1	1.0	C	55.78	55.67	39.28			
	WR	1	1.0	D	57.61	57.51	39.06			
	WR	1	2.0	A	62.68	62.44	38.93			
	WR	1	2.0	AB	71.78	66.22	39.12	32.66		27.10
Big Rock Ridge slide 1	BRR	1	1.0	A	49.96	49.93	39.05	10.91		10.88
	BRR	1	1.0	CD	52.20	52.17	38.80	13.40	1.66	13.37
	BRR	1	1.0	EF	63.77	63.67	38.86	24.91	1.82	24.81
	BRR	1	1.0	GH	56.84	56.62	39.12	17.72	1.42	17.50
	BRR	1	1.0	IJ	48.28	48.21	38.80	9.48	1.28	9.41
Walker Ranch Slide 3	WR	3	1.0	AB	51.58	51.32	38.63	12.95	1.35	12.69
	WR	3	1.0	CD	52.53	52.20	38.73	13.80	1.40	13.47
	WR	3	1.0	EF	56.33	55.72	38.81	17.52	1.32	16.91
	WR	3	1.0	GH	54.97	54.55	39.18	15.79	1.82	15.37
	WR	3	1.0	IJ	55.01	54.57	38.40	16.61	1.71	16.17
	WR	3	1.0	KL	56.09	55.65	39.01	17.08	1.84	16.64
Stubbs Vineyard	SV	1	1.0	AB	48.23	48.20	38.78	9.45	1.40	9.42
Slide 1	SV	1	1.0	CD	54.74	54.65	38.83	15.91	1.36	15.82
	SV	1	1.0	EF	50.24	50.19	38.90	11.34	1.48	11.29
	SV	1	1.0	GH	54.23	53.51	38.74	15.49	1.72	14.77
	SV	1	1.0	IJ	57.50	56.53	39.01	18.49	1.75	17.52
	SV	1	1.0	KL	59.37	58.07	38.81	20.56	1.75	19.26
Briones Crest Trail	BCT	1	1.0	AB		36.49	21.35			15.14
Slide 1	BCT	1	1.0	CD		34.89	21.35			13.54
	BCT	1	1.0	EF		42.05	21.35			20.70
	BCT	1	1.0	GH		37.92	21.35			16.57
Briones Crest Trail	BCT	2	1.0	AB		38.19	21.35			16.84
Slide 2	BCT	2	1.0	CD		43.22	21.35			21.87

Location	Volume from CloudCompare (cm3)	Dry Bulk Density (g/cm3; +/- 2%)	Average Dry Bulk Density (g/cm3)	depth (m)	Runout Distance (m)	% water	Debris Flow or slump
Walker Ranch Slide 1							Debris Flow
							Debris Flow
							Debris Flow
				0.30			Debris Flow
				0.00	104	17.02%	Debris Flow
Big Rock Ridge slide 1				0.34	30	0.28%	Debris Flow
	8.091	1.65	1.532	0.34	30	0.25%	Debris Flow
	13.726	1.81	1.532	0.34	30	0.42%	Debris Flow
	12.508	1.40	1.532	0.55	30	1.27%	Debris Flow
	7.414	1.27	1.532	0.55	30	0.75%	Debris Flow
Walker Ranch Slide 3	9.613	1.32	1.531	0.50	226	2.05%	Debris Flow
	9.840	1.37	1.531	0.50	226	2.45%	Debris Flow
	13.240	1.28	1.531	0.50	226	3.61%	Debris Flow
	8.690	1.77	1.531	1.15	226	2.73%	Debris Flow
	9.736	1.66	1.531	1.15	226	2.72%	Debris Flow
	9.284	1.79	1.531	1.15	226	2.64%	Debris Flow
Stubbs Vineyard	6.734	1.40	1.529	0.30	25	0.32%	Debris Flow
Slide 1	11.680	1.35	1.529	0.30	25	0.57%	Debris Flow
	7.677	1.47	1.529	0.30	25	0.44%	Debris Flow
	8.989	1.64	1.529	0.80	25	4.87%	Debris Flow
	10.540	1.66	1.529	0.80	25	5.54%	Debris Flow
	11.725	1.64	1.529	0.80	25	6.75%	Debris Flow
Briones Crest Trail	15.099	1.00	1.494	0.10			Slump
Slide 1	11.291	1.20	1.494	0.23			Slump
	11.244	1.84	1.494	0.28			Slump
	8.564	1.93	1.494	0.28			Slump
Briones Crest Trail	18.998	0.89	1.287	0.10			Slump
Slide 2	15.888	1.38	1.287	0.28			Slump

Location	Reason for Exclusion
Walker Ranch Slide 1	missing data & preliminary measurement
	preliminary measurement
	preliminary measurement
	preliminary measurement
	missing data
Big Rock Ridge slide 1	preliminary measurement
	preliminary measurement
	preliminary measurement
	preliminary measurement
	preliminary measurement
Walker Ranch Slide 3	preliminary measurement
	preliminary measurement
	preliminary measurement
	preliminary measurement
	preliminary measurement
	preliminary measurement
Stubbs Vineyard Slide 1	preliminary measurement
	preliminary measurement
	preliminary measurement
	preliminary measurement
	preliminary measurement
	preliminary measurement
Briones Crest Trail Slide 1	bedrock failure
	bedrock failure
	bedrock failure
	bedrock failure
Briones Crest Trail Slide 2	bedrock failure
	bedrock failure

Location	Loc	Slide	site	sample	mass (g) field capacity sample & container	mass (g) after bake sample and container	Mass container(g)	Mass Sample Field Capacity (g)	Bulk Density Field (g/cm3; +/- 2%)	Mass Dry Sample (g)
	BCT	2	1.0	EF		45.42	21.35			24.07
	BCT	2	1.0	GH		45.05	21.35			23.70
Highway 280	280	1	1.0	AB	46.09	41.91	21.35	24.74	1.33	20.56
	280	1	1.0	CD	54.26	49.05	21.35	32.91	1.79	27.70
	280	1	1.0	EF	45.96	42.55	21.35	24.61	1.18	21.20
	280	1	1.0	GH	43.88	39.70	21.35	22.53	1.43	18.35
	280	1	1.0	IJ	47.59	42.75	21.35	26.24	1.68	21.40
	280	1	1.0	KL	42.63	39.37	21.35	21.28	1.66	18.02
White Hill Slide 2	WH	2	1.0	GH	55.87	50.01	21.58	34.29		28.43
Twin Peaks Slide 1	TP	1	1.0	AB	51.32	46.59	21.95	29.37	1.38	24.64
Walker Ranch Slide 2	WR	2	2.0	IK	69.60	65.50	38.62	30.98		26.88

Location	Volume from CloudCompare (cm3)	Dry Bulk Density (g/cm3; +/-2%)	Average Dry Bulk Density (g/cm3)	depth (m)	Runout Distance (m)	% water	Debris Flow or slump
	16.122	1.49	1.287	0.54			Slump
	17.038	1.39	1.287	0.61			Slump
Highway 280	18.539	1.11	1.263	0.00			Slump
	18.410	1.50	1.263	0.05			Slump
	20.772	1.02	1.263	0.00			Slump
	15.744	1.17	1.263	0.03			Slump
	15.627	1.37	1.263	0.06			Slump
	12.791	1.41	1.263	0.12			Slump
White Hill Slide 2			1.253	0.51	172	17.09%	Debris Flow
Twin Peaks Slide 1	21.236	1.16	1.553	0.00			Slump
Walker Ranch Slide 2			1.405	0.70	27	13.23%	Debris Flow

Location	Reason for Exclusion
	bedrock failure
	bedrock failure
Highway 280	bedrock failure
	bedrock failure
	bedrock failure
	bedrock failure
	bedrock failure
	bedrock failure
White Hill Slide 2	missing data
Twin Peaks Slide 1	sampling error
Walker Ranch Slide 2	missing data